Synthesis, Characterization and Photocatalytic Activity of Transition Metal Vanadates Based Nanocomposites

Nazia Fakhar

Regn # 117270

A dissertation submitted in partial fulfillment of requirements

for the Degree of Master of Science in

Chemistry

Supervised by: Dr. Muhammad Fahad Ehsan

Co-Supervised by: Dr. Azhar Mehmood

Department of Chemistry

School of Natural Sciences

National University of Sciences and Technology

H-12, Islamabad, Pakistan

2017

FORM TH-4

National University of Sciences & Technology

MS THESIS WORK

We hereby recommend that the dissertation prepared under our supervision by: NAZIA FAKHAR, Regn No. 00000117270 Titled: Synthesis, Characterization and Photocatalytic Activity of Transition Metal Vanadates Based Nanocomposites be accepted in partial fulfillment of the requirements for the award of **MS** degree.

Examination Committee Members

1. Name: Prof. Habib Nasir Signature: _____

2. Name: Dr. Muhammad Arfan Signature: _____

External Examiner: Dr. Muhammad Naeem Ashiq Signature: _____

Co-Supervisor: Dr. Azhar Mahmood Signature: _____

Supervisor's Name: Dr. M. Fahad Ehsan Signature: _____

Head of Department

31-10-2017
Date

COUNTERSINGED

Date: 31/10/17

Dean/Principal

THESIS ACCEPTANCE CERTIFICATE

Certified that final copy of MS thesis written by **Ms. Nazia Fakhar**, (Registration No. **00000117270**), of **School of Natural Sciences** has been vetted by undersigned, found complete in all respects as per NUST statutes/regulations, is free of plagiarism, errors, and mistakes and is accepted as partial fulfillment for award of MS/M.Phil degree. It is further certified that necessary amendments as pointed out by GEC members and external examiner of the scholar have also been incorporated in the said thesis.

Signature: _____

Name of Supervisor: Dr. M. Fahad Ehsan

Date: _____

Signature (HoD): _____

Date: 31-10-2017

Signature (Dean/Principal): _____

Date: 31-10-17

Dedicated to

my loving parents

for their endless love, support and encouragement

Acknowledgements

*All praise to the great **Allah Almighty** who has bestowed me with the opportunity to seek knowledge and enabled me to fulfill the obligation to explore the world of science up to my maximum limits. Without Allah Almighty's will, all this would not have been possible.*

*I would like to express my sincere gratitude to my **research supervisor Dr. Muhammad Fahad Ehsan** for his motivation, continuous support, patience and immense knowledge. He has guided me completely through- out my research work. Working under his supervision has indeed broadened my vision.*

*Besides my supervisor, I would like to thank my co-supervisor **Dr. Azhar Mehmood** for always being available in the time of need, his encouragement and insightful comments.*

*I am also really thankful to my GEC members, **Prof. Dr. Habib Nasir (HoD Chemistry)** and **Dr. Muhammad Arfan** for sparing precious time from their busy schedules, for their constructive criticism, suggestions as well as moral support. I am indeed indebted to **Prof. Dr. Habib Nasir** for his unlimited support, valuable advice and guidance in my research work. Besides this I would like to thank the SNS faculty for being extremely cooperative especially **Sir Ishrat, Sir Moazzam** and **Sir Tanveer**.*

*A special thanks to my friends and group members, without whom this journey would not have been this amazing. I am very thankful for the love and prayers of **Zainab Qayyum, Farea Batool, Amna Akram, Syeda Farrah Naz, Maham Akhlaq** and **Amna Ashraf.***

*Last but not the least, I would pay my regards to my **parents** for their un-parallel love and spiritual support throughout my life and my **siblings** for their encouragement throughout my research work.*

Nazia Fakhar

Table of Contents

Table of Figures

Table of Tables

Abstract:

As a result of industrial revolution, a remarkable increase has been observed in the global energy utilization and environmental pollution. Currently, major energy requirements are being fulfilled by non-renewable energy sources. Renewable energy sources are gaining popularity with time, because of being an infinite source of energy, cost effectiveness etc. World is facing severe energy and environmental crisis, and majorly the organic effluents from industrial wastes are damaging environment to an alarming degree. Water pollution, a major type of pollution, is a cause of various potential acute health diseases and potential chronic health diseases. Contaminants must be decomposed to smaller levels before disposal, so that they are not harmful to humans and the environment. Various methods used for the removal of toxic organic pollutants include biological, physical and chemical methods. Among the available chemical methods, heterogeneous photocatalytic oxidation is an effective method for the degradation of large number of persistent organic pollutants. Semiconductor based photocatalysts are commonly used materials for the photodegradation of organic pollutants and toxic dyes. Factors that affect the efficiency of a photocatalytic system include nanostructuralization, doping, heterostructure formation, sensitization etc. Here, use of $Zn_3V_2O_8$/$Co_3V_2O_8$ and $Co_3V_2O_8$ /g-C_3N_4 for photocatalytic dye degradation has been discussed. Co-precipitation method has been used for the synthesis of UV light active $Zn_3V_2O_8$ and visible light active $Co_3V_2O_8$ nanoparticles. Thermal decomposition method has been used for the synthesis of g-C_3N_4. Both $Zn_3V_2O_8$ and $Co_3V_2O_8$ have orthorhombic geometry, and the composite shows good photocatalytic efficiency towards the degradation of Congo red which is upto 70%. Photocatalytic activity of nanocomposites of cubic g-C_3N_4 and orthorhombic $Co_3V_2O_8$ was investigated against congo red, a high %age efficiency i.e. 86% for dye degradation was obtained. Different techniques were used for the characterization of as-synthesized photocatalysts. Crystal structure, morphology, purity, composition and band gaps of photocatalysts and their heterostructures were studied by XRD, IR, SEM/EDX, and UV-Vis. DRS, UV-Vis absorption spectroscopy

.

Literature Survey

Abstract

This chapter provides a detailed account of the energy and environmental crisis, possible solutions to encounter the increasing environmental pollution. It basically focuses on the use of semiconductor based photocatalytic materials for the removal of toxic pollutants. Photocatalysis used for the degradation of organic dyes, mechanism of photocatalysis, followed by the different factors for the enhancement of photocatalysis have been extensively discussed in this chapter. Last part of the chapter comprises the objectives, motivation and scope of the research that has been carried out.

1.1 Introduction

Modern era is an era of technology and industrialization. Nowadays, natural resources are extensively being used in order to meet the energy needs of the present time. This, in turn is, resulting in the depletion of the natural i.e. environmental resources. In order to cope up with the energy issues and the environmental hazards, rapid measures are required to be taken.

1.1.1 Energy Infrastructure

As a result of industrial revolution, a remarkable increase has been observed in the global energy utilization. Fossil fuels have been excessively used to fulfill the energy demands. According to a survey, it has been reported that in 2015, the major contributors of the energy sources mainly included carbon rich fossil fuels i.e., oil (32.94 %), coal (29.20%), gas (23.85%) and nuclear energy (4.44%). Renewable energy resources contributed 9.57% to the global energy consumption and among these, hydro had been the major contributor. **Fig. 1.1** comprises the major energy contributors along with their percentage contribution till 2015.

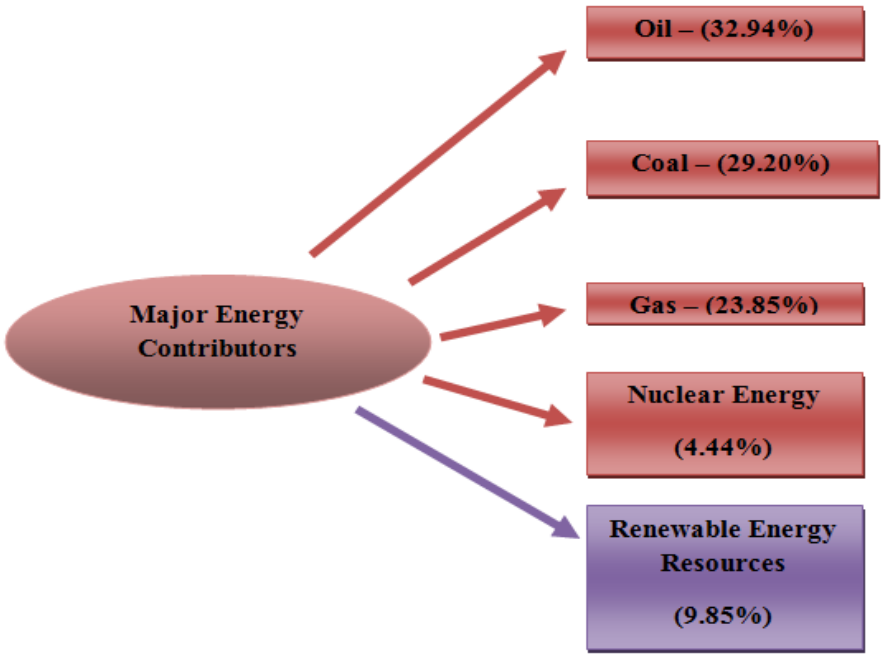

Figure 1.1 Major energy contributors till 2015

Over the years, fossil fuels have promised to be an efficient energy source. It has been reported that, till 2005, fossil fuels contributed 93.19% of the total energy demand whereas, by 2010, the energy contribution by fossil fuels have been 92.17%, and by 2015 the energy contribution has decreased to 90.43%. But still, fossil fuels are the major contributors towards the global energy demand and would be of great importance in the near future as well.

1.1.1.1 Non-Renewable Energy Resources

Non-renewable energy resources are the most excessively used sources of energy in the current time. Most prominent non-renewable source of energy includes fossil fuel. Three main types of fossil fuels include coal, oil and natural gas. Currently, more than 90% of the energy demands are being fulfilled by the use of fossil fuels. Hence, they have proved economical to mankind in several ways. Following are the factors that make fossil fuels a promising energy source.

Abundantly available Though the renewable energy resources are gaining popularity with time, still the most commonly used energy source is the fossil fuels. Common usage of the fossil fuels

is greatly attributed to its abundant availability. Plenty of places in the world are rich in fossil fuels. Fossil fuels have been meeting the energy demands since decades, and still the world can rely on these energy sources for a further few decades.

Easy Set Up Renewable energy resources, even being infinitive, have dependency on wind, water, sun. Whereas, fossil fuels are easily and widely available. Large quantities of fuel can be generated by setting a single fossil fuel plant, anywhere in the world. Energy in huge amount can be produced easily from a single fossil fuel plant. Energy generated from fossil fuels can be stored and transported easily.

Safe to Transport Owing to the high stability of fossil fuels, their transportation from one place to another is quiet easy. Among all the energy sources, fossil fuels are the easiest to transport. Large trucks can be used for their transportation. Besides this, large pipelines above or below the ground can be used for the efficient pumping of fossil fuels. Above all, their modes of transportation are economical

Low Cost In comparison to the other energy sources, the setup, extraction, refinement and transportation of fossil fuels is the cheapest. Besides this, fossil fuels also find the advantage of "pre-existing". Fossil fuels are a prominent energy source because of their efficient energy production and low cost.

Stability Primary components that make up the fossil fuels include carbon and hydrogen. Both these elements show high degree of stability and do not show chemical conversion into some new compound. Excess of carbon present in fossil fuels make it stable and productive. Despite being the most efficient energy source, nuclear energy consists of radioactive elements that are unstable.

High Calorific Value Total amount of energy present in any fuel refers to its calorific value. This energy is produced in the form of heat, which is produced by burning and combustion of fuel. Calorific value has a direct relation with the efficiency of the material. Fossil fuels are said to have the highest calorific values among the fuels, making them the most prominent source of energy.

Higher energy production High efficiency of fossil fuels results in greater energy production. Energy obtained by burning a small amount of fossil fuels i.e., coal, oil etc. is far greater than the energy obtained from any other source. This aspect makes fossil fuel most popular and reliable source of energy. Industrial revolution owes to the high efficiency of fossil fuels [11].

Limitations of fossil fuels

Irrespective of the large number of advantages of fossil fuel, consumption of fossil fuels also account for certain alarming limitations. The cons of using fossil fuels as an energy source are discussed below:

Non-renewable Rapid consumption of fossil fuels is leading towards their depletion. The most prominent limitation of using fossil fuels is that they are non-renewable. Fossil fuels are a finite source of energy. A finite amount of fossil fuels is present, and once used, it will require centuries to rebuild them. Being non-renewable, a drastic increase in the price of fossil fuels is expected in the near future [1].

Environmental Pollution Combustion of crude oil produces environmental pollutants. Burning of fossil fuels result in the direct release of CO_2 into the atmosphere. Hence, fossil fuels cause environmental pollution. CO_2 is a major greenhouse gas which is resulting in global warming. Burning of fossil fuels is affecting the aquatic as well as the life on land, equally. Increase in the combustion of fossil fuels is increasing the levels of CO_2 in atmosphere. Radical changes are expected if this trend prevails

Acid Rain Burning of fossil fuels results in the production of CO_2 and SO_2. Sulphur dioxide is responsible for acid rain. It gets accumulated in the upper atmosphere. With the very first rain, these gases react with water and this rain is known as acid rain. Acid rain acidifies the loams, destroying the crops. It also causes the destruction of marble and brick-work of monuments. Acid rain is also responsible for various skin and respiratory diseases.

Oil Spill Heavy transportation for fossil fuels is required in order to set up the power stations. Transportation and shipping may result in some crucial accident. These accidents result in

disposal of oil on land or in water. The toxic substances present in the crude oil reserves are equally dangerous to any form of life. Oil spills are not common, but once they occur they can engulf hundreds of lives.

Health Issue Toxic gases produced as a result of burning of fossil fuels is causing ozone hole. The depleted ozone layer allows the ultra-violet radiations to reach the earth's surface. These UV rays are harmful and are responsible for skin cancer and eye disease [4].

1.1.1.2 Renewable Energy Resources

Energy that is generated by using natural resources is known as renewable energy.. Because of the continuous depletion and limitations of fossil fuels, environment friendly and renewable energy sources are needed to be explored. Different renewable energy sources include biomass, wind, geothermal, hydrothermal and solar energy [2, 3], which have been pictorially illustrated in **Fig. 1.2.**

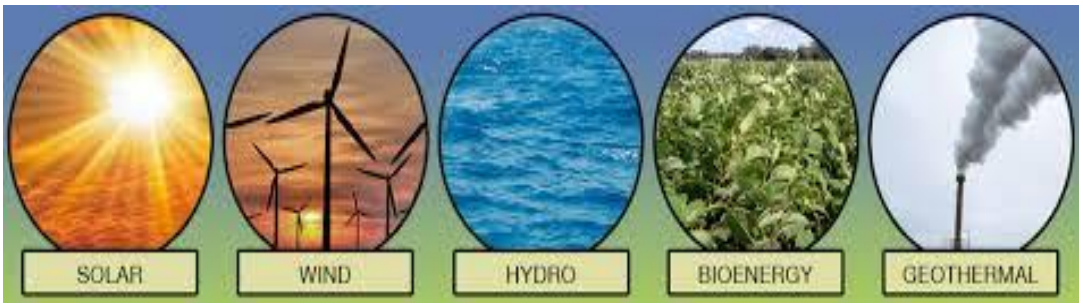

Figure 1.2 Renewable energy sources

Biomass Organic material that originates from plants is known as biomass. Here, basically photosynthesis is used to collect and store the solar energy. Biomass energy, also known as bioenergy, involves the conversion of biomass to different forms including fuel, electricity, heat etc., as a result of combustion of plants. Direct use of energy crops can be done to obtain biomass. Residue that is generated during the processing of crops also contributes to biomass. Biofuels are the intermediate energy carriers obtained from biomass and these may include ethanol (liquid fuel), charcoal (solid fuel having high energy density) or producer gas. A considerable variation is observed in the percentile contribution of biomass every year, but the contribution from biomass is high i.e., 100-300 EJ annually [5].

Wind Kinetic energy is produced as a result of movement of air from one place to another, and this kinetic energy is referred to as the wind energy. Wind mills and wind turbines are used for the conversion of wind energy into mechanical and electrical energy. Wind energy is produced as a result of energy obtained from the sun in the form of heat. Heat produced from sun warms up the air on the surface of land. Hot air being lighter is replaced by the denser cold air, and the hot air moves to the upper atmosphere. In this way, wind keeps on moving and energy is generated. In this way, energy produced from wind proves to be an economical, abundant and renewable energy source.

Water It is the most abundantly used source of renewable energy. Hydro energy is of three different types including hydroelectric energy, wave energy and tidal energy. The latter two vastly come under the ocean energy. Turbines are used to convert the gravitational potential energy of falling water into different types of energy and this phenomenon comes under the hydroelectric energy. In oceans, the tides move and the energy produced as a result is known as tidal energy. Waves are produced as a result of wind, the energy thus generated is used to move turbines and this results in the generation of electricity. Electricity is generated as a result of conversion of retained potential energy into kinetic energy, as a result of flow of water with high speed and this conversion is carried out by shafts and turbines [6].

Geothermal Heat energy from the earth is known as the geothermal energy. The source of geothermal energy includes the magma. Magma is hot and molten layer of rock present beneath the earth's crust. Naturally radioactive materials (potassium and uranium) present beneath the crust decay and heat energy is produced. Heat present within 33,000 feet of earth contains 50,000 times greater energy than the non-renewable energy sources. Hot spots are the regions with the highest geo-thermal energy. Another source of geo-thermal energy involves the natural hot springs. Rock covering breaks as a result of earthquakes and the movement of magma. This, in-turn results in the circulation of water and natural hot springs occur when the water rises to the surface. Here, the temperature of water can be more than 200^{o}C. The geo-thermal energy is captured by using natural hydrothermal convection systems. Here, cold water seeps into the

earth, gets heated up and then rises to the earth's surface. After it, the steam is captured and electric generators are driven.

Solar The most abundant and important source of renewable energy is sun. Solar energy is clean and can be utilized independently. Solar panels use semiconductor materials (p-type and n-type) for the conversion of solar light into usable forms of solar energy. The phenomena of electricity production is as the light falls on the surface of semiconductor, flow of electrons occur, thereby converting photons into voltage and this is known as photovoltaic effect Photovoltaic and thermal systems are the major types of solar energy systems used nowadays. Conversion of solar energy into electricity is carried out by using photovoltaic systems. When light falls on silicon panels, electricity is generated. In solar thermal systems, heat from the sun is stored and then is used to produce energy [7, 8].

In order to cope up with the environmental issues, solar fuel (H_2, methane, methanol etc.,) is generated by converting solar energy into chemical energy. Current and the future energy demands can be fulfilled by effective harvesting and storage of the solar energy. Use of renewable energy sources is increasing with time and it seems that solar energy would prove to be the most prominent renewable energy source in the near future. Researchers have devised new procedures to convert CO_2 and H_2O directly into fuel, by the use of solar energy. Nowadays, solar energy is successfully being used for the removal of environmental pollutants. Industrial wastes, mainly comprising the hazardous effluents and organic waste are treated with the help of sunlight. Ong et al. reported hexagonal ZnO nanoparticles for the photocatalytic degradation of Congo red. Different solvents were used for the synthesis of ZnO nanoparticles via sol-gel method, and particles with an average crystallite size of 23nm were synthesized. The percentage dye degradation of up to 77% was reported [73]. Erdemoglu et al. studied the Congo red degradation under visible light, using anatase TiO_2 nanoparticles with an average size of 8nm. The photocatalyst was synthesized successfully via hydrothermal route. Efficiency of TiO_2 nanoparticles was studied by taking various factors in account, such as irradiation time, pH, initial dye concentration etc. Finally the degradation products were analyzed using LC-MS technique [74].

1.2 Energy and Environmental Crisis

Limited natural resources, used to power the industrial society are depleting with the increase in energy demands. A finite availability of the natural resources is a major concern to fulfill the energy needs, in near future. Energy crisis are a result of overconsumption of natural resources, overpopulation, poor infrastructure, unexplored renewable energy sources, wastage of energy, natural calamities and accidents, wars etc. To overcome the energy crisis, we need to shift towards renewable energy sources.

Environmental crisis is a dramatic, irreversible worsening of the environment. Major environmental problems include pollution, global warming, overpopulation, depletion of natural resources, climate change, loss of biodiversity, deforestation, ocean acidification, ozone layer depletion, acid rain, **water pollution,** urban sprawl, genetic engineering etc. Water pollution is major environmental issue, which is threatening human and animal life equally [9].

1.2.1 Water Pollution

Contamination of water bodies i.e. oceans, river, lakes, ground water, aquifers etc. refer to water pollution. Toxic pollutants in water resources are increasing day by day, affecting flora and fauna. Causes of water pollution may include industrial waste, sewage water, mining activities, marine dumping, accidental oil leakage, burning of fossil fuels, chemical wastes, radioactive waste, toxic **organic dyes** etc.

Textile waste water

Variety of dyes and chemicals are the major components of textile waste water. Dyeing and finishing processes contribute largely towards the toxification of water used in textile industry. Dye material usually comprises complex organic compounds, lethal to any form of life. The principle medium used to apply dyes and chemicals for finishes is water, hence dyes and colors are major water pollutants [10]. Textile waste water containing high content of toxic organic dyes is enrich in color, metals, sulphides, surfactants, organic processing agents etc. Different types of dyes include natural dyes, synthetic dyes and food dyes. Azo dyes are the commonly used coloring agents and constitute about 70% of the organic dyes produced per year [11].

Market demand of dyes is increasing day by day, so proper disposal and degradation of toxic dyes is of consideration. Dyes used in textile industry are classified as:

a) Acidic Dyes
b) Basic Dyes
c) Neutral Dyes

Use of synthetic dyes gained popularity by the mid of 19^{th} century. Mauveine, also known as Perkin's mauve and aniline purple, discovered in 1856, was the first synthetic dye. These dyes contain carcinogenic compounds, e.g., different aromatic compounds, benzidine, naphthalene etc. therefore their proper disposal is of immediate concern [12, 13]. Dyes may show high stability towards heat, light, chemicals etc. making their biodegradation a difficult task [14].

1.2.2 An Introduction to Dyes

Dye is an ionizing, colored and aromatic organic compound, possessing high affinity against the substrate. Coloring can be used to identify the individual components of a tissue section. Dyes are extensively used in textile, paper, leather and plastic industry. Dyes may show similar behavior as that of chemicals, as dyes can be toxic, mutagenic and carcinogenic. Thereby, posing a severe threat to human and aquatic life. Major break-through in the history of dyes was reported in 1856, as a result of an accidental synthesis of Aniline Mauve dye. This dye has been named after non-fast color, derived from natural dyes. Mauve, a basic and first synthetic dye, is a derivative of coal-tar [75].

Major Constituents of Dyes

Dyes appear as colored substance because of the presence of **chromophore**. Dyes basically comprise aromatic rings. The structure of dyes consists of aryl rings that have an extensive delocalized electron system. Depending upon the energy of the electron cloud, these aromatic rings absorb light of different wavelength (from the visible region of electromagnetic spectrum). Chromophores make the energy changes in the electron cloud of dye molecule, and these energy changes are responsible for the absorption of light in visible region of the spectra. Human eye detects the absorptions and reflections made in visible region. Removal and localization of electrons from the electron cloud result in loss of color of the dye molecule. As a result of

removal of electrons, the remaining electrons revert to the orbits. For example, in case Schiff's reagent the ring ceases to act as a chromophore because of the localization of electrons. Hence, chromophores have delocalized electrons, having alternate double and single bonds [76, 77].

The color of dyes can be altered by the addition of modifiers. Methyl and ethyl groups act as modifiers. Color change follows the mechanism of energy alteration of delocalized electrons. It is properly explained according to methyl violet series.

- Original dye (Pararosanil), with no methyl group is red in color

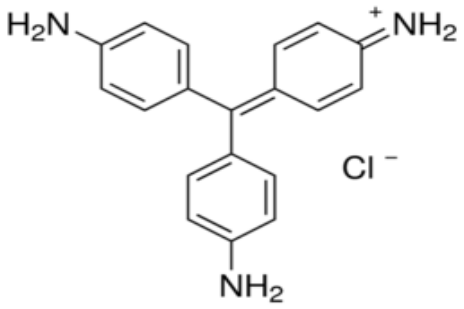

- Methyl violet is a reddish purple dye, with four methyl groups in its structure [78]

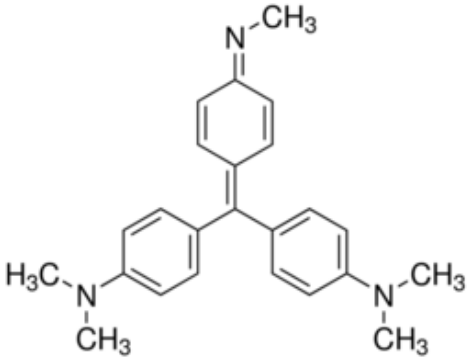

- Crystal Violet is a purple blue dye, obtained by the addition of six methyl groups to the original dye [79].

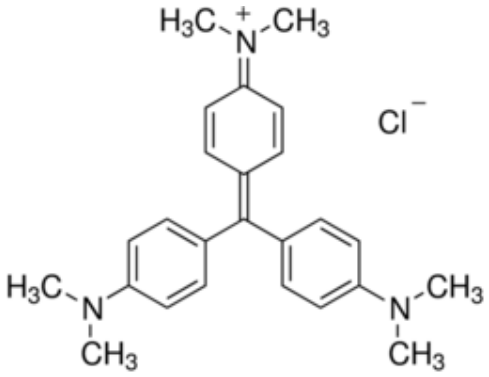

- Methyl green is obtained by the addition of seven methyl groups to the original dye molecule [80].

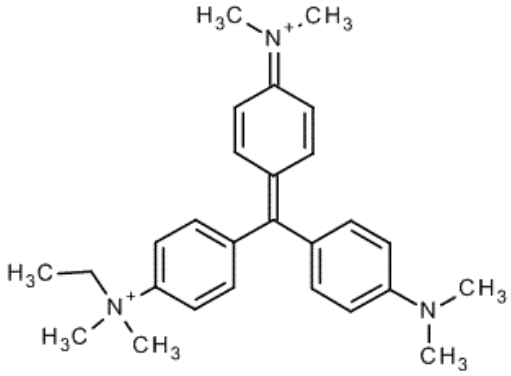

Auxochrome is another major component of dye molecule, which imparts cohesiveness and stability to the dye molecule. Auxochrome can also intensify the color. Auxochromes are a group of atoms attached to the non-ionizing compounds, still having the ability to ionize. Positively charged and negatively charged are the two types of auxochromes. Different examples of auxochromes include:

--OH, --NHR, --Cl, --Br, $--CH_3$, $--NO_2$, $--NR_2$, --COOH, $--NH_2$, $--SO_3H$

Classification of Dyes

Different classes of dyes differ from each other in their unique chemistry, particular way of bonding and structure. Some dyes react chemically, while the others just undergo physical interaction. Prominent ways for the classification of dyes may include:

- Organic/Inorganic

- Natural/Synthetic
- By area and method of application
- By the nature of electronic excitation
- According to dyeing technique (anionic, disperse, direct)

Besides these, dyes can also be classified into acidic, basic and neutral dyes [81,82].

Acidic Dyes. These dyes are negatively charged and bind to positively charged molecules. Acidic dyes are also known as anionic dyes. Examples include Nigrosine, india ink, congo red, acid fuschin.

Basic Dyes. These are positively charged dyes and bind to negatively charged species. Basic dyes are also known as cationic dyes. Common examples include basic fuschin, crystal violet, methylene blue, safranin etc.

Neutral Dyes. Acidic and basic dyes combine and precipitate, resulting in the formation of neutral dyes. They include giesma stain, eosinate of methylene blue etc.

Dyes as Hazardous Materials

Some of the dye constituents e.g. Hematoxylin and hematin are harmful if inhaled, absorbed through skin or ingested. Inhalation of bloodroot can cause inflammation and irritation. In case of natural dyes, mordants that are used can also affect human health. Dyes affect the absorption and reflection of sunlight in water. Hence, it diminishes the photosynthesis in algae, and also disturbs the food chain. Mostly the dyes and their breakdown products are carcinogenic and mutagenic. Dyes affect the transparency and quality of water bodies. Decrease in light penetration causes oxygen deficiency, thereby causing severe damage to aquatic life. Reactive dyes are a cause of respiratory diseases, asthma, contact dermatitis and allergic dermatoses in humans. Exposure to textile industry leads towards severe changes in immunoglobulin level, genotoxicity and mutagenicity. Even very low concentration of these dyes can prove to be extremely harmful [83].

Industrial effluents are the major source of introducing toxic dyes to the environment.

1.2.3 Methods for the Removal of Toxic Dyes from Waste Water

Azo dyes are major water pollutant, hence removal of dyes is of major concern. Efficient color removal can be carried out by using different methods.

- Physical Methods
- Electrochemical Methods
- Biological Methods
- Chemical Methods

Physicals Methods

Different physical methods used for the removal of toxic dyes include adsorption, flocculation-coagulation, membranes, irradiation, ion-exchange etc. Adsorption is the most common physical method used for dye removal. Activated carbon is a widely used adsorbent for a variety of dyes. Magnetic nanomaterials (Iron oxide, Nickel oxide, Nickel Cobaltite, Cobalt ferrite etc.) are extensively used for adsorption these days. Coagulation-flocculation technique decolorizes the textile effluents and reduces organic content. Membrane filtration clarifies, concentrates and then separates the dyes from effluent [15, 16].

Electrochemical Methods

Electrocoagulation and indirect oxidation are the two electrochemical methods used to separate dyes from waste water. Electrocoagulation technique uses direct current source, metal electrodes are dipped into the effluent and dissolved dyes get removed by precipitation or flotation. Indirect oxidation of the effluents can be carried out within an electrochemical cell, to get rid of the toxic dyes [17].

Biological Methods

Aerobic and anaerobic degradation, algae, fungi etc. can be used for the removal of colors from waste water [18, 19]. Mainly, the dissolved organic matter gets removed using biological methods. Efficiency of these methods is greatly dependent upon the ratio between the organic load (dye) and the microorganism concentration, temperature etc. [20].

Chemical Methods

Chemical treatment involves the use of chemicals for water treatment. Chemical methods used for dye removal include ozonation, advanced oxidative processes, neutralization, chlorination etc. High color and residual removal is carried out by ozonation [21]. Ozone is applied in gaseous state; hence it does not increase the volume of waste water. Short half-life of ozonation makes it a less important tool for water treatment. In advanced oxidation technique, OH radicals attack the chromogenic group, organic peroxide radicals form, which afterwards converts into less toxic material. Acid or base is added in water to neutralize, improving the quality of water [22]. Photochemical Methods are most commonly used methods for toxic dye removal, these days. A renewable energy source i.e. solar is used for degradation of organic dyes, thus making photocatalytic degradation more appropriate [23].

1.3 Photocatalysis

Photocatalysis is a Greek word, photo means "light" and catalysis means "decompose, break apart". Photocatalysis is a process which uses light to activate a substance i.e. photocatalyst, it modifies a chemical reaction without itself being chemically transformed. Thermal catalyst differs from photocatalyst, as a thermal catalyst is activated by heat whereas; photons of appropriate energy are used to activate a photocatalyst. A photocatalyst absorbs photons, generates electron-hole pairs, which then degrades the pollutants into less toxic material. A natural photocatalyst i.e. chlorophyll converts CO_2 and H_2O into glucose and oxygen [24, 25].

Photocatalysis plays a vital role in order to cope up with the energy and environmental crisis. Commonly used photocatalyst for environmental remediation include semiconductor photocatalysts. These materials absorb solar energy and generate electrons and holes. These charge carriers carry out the oxidation and reduction of toxic environmental pollutants and convert them into CO_2 and H_2O. A suitable photocatalyst possesses large surface area, favorable band-gap, appropriate morphology and can be reused [26]. Extensively used semiconductor based photocatalysts, used for the degradation of environmental pollutants, along with their band-gap energies have been illustrated in **Fig 1.3.**

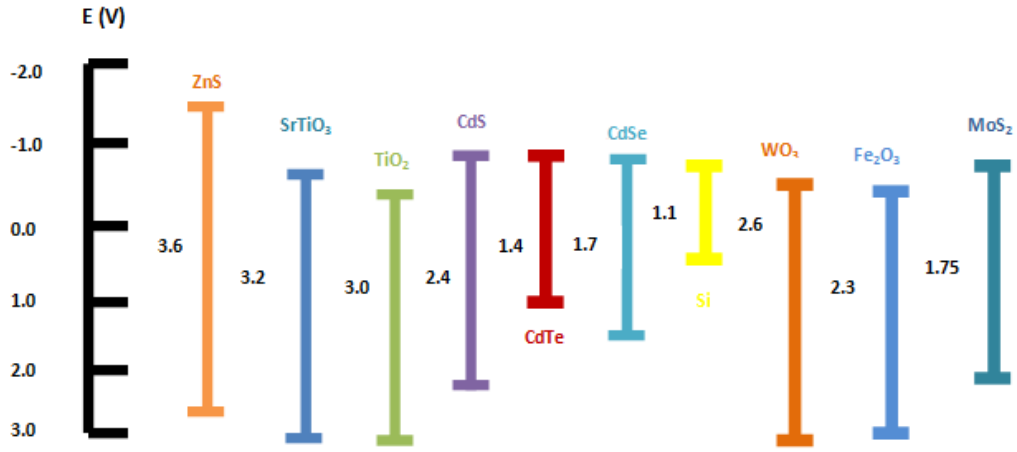

Figure 1.3 Schematic illustration of band gaps and redox potential of various semiconductors at pH=1 (vs. NHE)

1.3.1 Types of Photocatalysis

Photocatalysis is of two types

- Homogeneous Photocatalysis
- Heterogeneous Photocatalysis

Homogeneous Photocatalysis

Reactants and photocatalyst, when present in same phase, refers to the homogeneous photocatalysis. Photo-fenton systems and ozone are the commonly used homogeneous photocatalysts [27].

Heterogeneous Photocatalysis

Photocatalysis, in which reactants and photocatalyst are in different phases, is known as heterogeneous photocatalysis. In it, an interface forms between the solid photocatalyst and the liquid containing the precursors and the product. In heterogeneous photocatalysis, the solid photocatalyst is either in contact with a liquid or a gaseous phase. Photocatalyst usually consists of a semiconductor material, which absorbs the photons. Photocatalytic reactions (oxi and red),

takes place at the interface between the gas/liquid and semiconductor photocatalyst. Heterogeneous photocatalysis finds application in energy and environment related applications, organic synthesis etc. [28]. As a result of photocatalysis, organic waste gets converted into less toxic material. Heterogeneous photocatalysis is a cost effective method, for the degradation of environmental pollutants [29].

1.3.2 Mechanism of Photocatalysis

When a photon, having energy equal to greater than the band-gap energy of the photocatalyst, is absorbed by the material, excitation of an electron occurs from the valence band of a material to its conduction band, this phenomena is known as photocatalysis. Generation of the photogenerated charge carriers is a prerequisite step in all photocatalytic processes. Electrons and holes tend to recombine and give away energy as heat. However, an electric field generates at the semiconductor-metal or semiconductor-fluid interface, which decreases the rate of recombination. In this way, lifetime of the charge carriers increase and subsequently charge transfer occurs between the species and a chemical reaction initiates. Interfacial electron transfer is the most critical step in photocatalytic process, as it deals with the transfer of electron between the substrate and the semiconductor photocatalytic material. Efficiency of the electron transfer reactions depend upon the position of semiconductor's valence and conduction band to the redox potential of the adsorbed material. In order to carry out a photocatalytic reaction, the conduction band of the electron acceptor species should be more positive than the conduction band of semiconductor photocatalyst, whereas the valence band of the electron donor specie should be more negative than the valence band of semiconductor. As a result of interfacial electron transfer process, redox reaction takes place and product is obtained [30]**.** Hence, three main steps of semiconductor photocatalysis reaction can be stated as

- Transition of electrons from VB to CB, as a result of absorption of solar energy
- Transfer of the photogenerated charge carriers to the surface of photocatalyst
- Reaction between the transferred electrons/holes with the adsorbed electron acceptors and electron donors

A major problem encountered in the second step is the enhanced recombination. So, various strategies are opted to control or decrease the recombination of photogenerated charge carriers

[31]. Major steps involved to carry out the photocatalysis have been schematically illustrated in **Fig 1.4** Where (I) Light absorption(II) Charge separation, (III) Charge migration, (IV) Charge recombination and (V) Redox reactions

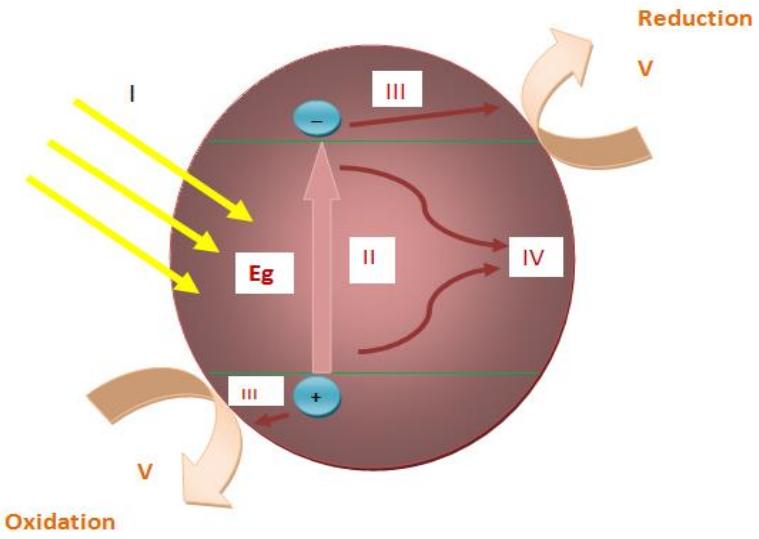

Figure 1.4 Steps involved in Photocatalysis

1.3.3 Semiconductor based Nanomaterial (Photocatalyst)

Unique physical and chemical properties of semiconductor nanomaterials make them promising material for photocatalytic applications. Different types of semiconductor materials used for photocatalytic dye degradation include metal oxides, metal nitrides, metal chalcogenides, carbon nitride etc. Essential problems in photocatalytic applications include efficient charge separation, use of an effective co-catalyst, visible light absorption etc. and these problems can be solved using various dimensional semiconductor nanostructures.. Nanostructured semiconductor photocatalysts show enhanced activity owing to their small size. Small size results in increased surface area and also increased reactive sites. But small material size can cause a decrease in photocatalytic activity as it may cause strong quantum confinement, thus increasing the probability of recombination. Recombination rate can be reduced by setting a concentration or potential gradient, which in turn is related to morphology, surface properties and structure of the nanomaterial. Formation of heterostructures greatly decreases the rate of recombination [33]**.** Main features of a photocatalytic system include desired band-gap, high surface area, reusability,

stability and suitable morphology. Metal oxides i.e. chromium, vanadium, zinc, cerium etc. have been reported for the photocatalytic dye degradation. Firstly light absorbs, which induces charge separation. The positive charge carriers (i.e. holes) oxidize the organic substrate and degrade the toxic dyes [32]. Photocatalytic activity of semiconductor material depends on two things.

- Generation of hydroxyl radical, as a result of oxidation of hydroxyl anions
- Generation of oxygen radical, as a result of reduction of oxygen

Abundantly studied semiconductor photocatalysts include, TiO_2, SnO_2, CeO_2, ZnO, which have been extensively used for the degradation of azo dyes (methyl blue, methylene orange, Rhodamine blue, Congo red etc.) [34].

In semiconductors, band-gap is characterized by a series of closely packed energy levels linked with covalently bonded atoms forming the valence band and another sequence of spatially diffused energy levels, giving rise to the conduction band. Band-gap is the energy difference between the conduction band and the valence band. Light absorption capacity of a semiconductor material is directly linked to its band-gap. Photocatalyst must be cost effective, environment friendly, abundantly available etc. A photocatalyst should possess a wide range of light absorption capacity, high charge mobility in order to prevent recombination. Interaction between the photocatalyst and adsorbed specie takes longer time to occur, as compared to the recombination rate of photogenerated charge carriers, therefore recombination rate is required to be decreased [35,36].

Metal oxides as Photocatalyst

Commonly used metal oxides for the degradation of organic pollutants include TiO_2, ZnO, SnO_2, SiO_2, ZnS, CoO etc. Besides these, vanadates are also emerging beneficial for various photocatalytic applications. Commonly used vanadates are bismuth vanadate, cobalt vanadate, zinc vanadate, iron vanadate etc. Metal oxides absorb energy in either ultraviolet region, visible region or both. Electrons gain energy on irradiation to sunlight and get transferred from the valence band to the conduction band, leaving behind holes. These charge carriers are responsible for the degradation of environmental pollutants.

TiO_2, SnO_2, ZnO as Photocatalysts: Alshammari et al. reported semiconductor photocatalyst i.e. Au-titania and Au.zincite for the photocatalytic removal of Rhodamine B under UV-A. Au supported zincite showed greater photodegradation than Au supported titania, because gold nanoparticles showed greater reflection to UV-light, over titania support [37].

Amini et al. synthesized hexagonal TiO_2 and ZnO nanoparticles having rutile phase. Photocatalytic degradation of methylene blue, Rhodamine B and acridine orange was carried out using the above mentioned metal oxides. A decrease in dye degradation was observed when ZnO was used, because ZnO is unstable and converts into $Zn(OH)_2$, leading towards catalyst inactivation [38]**.** ZnO doped SnO_2 nanoparticles have been reported for photocatalytic degradation of methylene blue. An electrostatic field is induced as a result of absorption of light. Electrons shifted from ZnO to SnO_2, whereas holes moved towards ZnO side. These photogenerated charge carriers in ZnO/SnO_2 heterojunction participated in the chemical reactions. Holes in the valence band react with adsorbed H_2O or OH- to produce OH radical, whereas the electrons in the C.B reduced O_2 to produce suoperoxide radicals etc. [39].

Ternary Metal oxides as Photocatalysts

Difference between ternary metal oxides and common metal oxides is that the former possesses sharp absorption edges. Here, 2p orbital of oxygen hybridizes with the orbitals of transition metals, which result in a decrease in band gaps of ternary metal oxides [84]. Ternary metal oxides are emerging as a new field for the removal of environmental pollutants. Commonly used ternary metal oxides used for photocatalytic dye degradation have been discussed below

Bismuth Vanadate ($BiVO_4$) as a Photocatalyst

Bismuth nitrate, bismuth chloride, ammonium metavanadate are the commonly used precursors for the synthesis of bismuth vanadate nanostructures. Bismuth Vanadate has a band-gap of 2.4eV, and is the most abundantly used vanadate for photocatalytic applications. Yan et al. reported novel $BiVO_4/Ag_3VO_4$ hetero-junction for the photocatalytic removal of rhodamine B, congo red, methyl blue, methyl violet and methyl red. Hydrothermal method was used for the synthesis of nanocomposite. 95.9% degradation of Rh-B was obtained, which was many times greater than pristine Ag_3VO_4 and $BiVO_4$. Heterojunction lead towards greater photocatalytic efficiency, because of the effective charge separation between electrons and holes [40]. Odling

et al. deposited $BiVO_4$ over TiO_2, using SILAR method. Visible light harvesting of TiO_2 film increased as a result of successive deposition of $BiVO_4$. This heterojunction had a type II band structure. Photocatalytic efficiency of the material was measured by carrying out the degradation of Rhodamine 6G. Mismatch of the valence band and conduction band energies results in reduced photocatalytic activity because of poor charge separation, which was observed in the case of $BiVO_4/ZrO_2$ composite [41].

Zinc Vanadate ($Zn_3V_2O_8$) as a Photocatalyst

Cubo-octahedral $Zn_3V_2O_8$ has been synthesized using $ZnSO_4$ and ammonium vanadate as precursors. $Zn_3V_2O_7(OH)_2(H_2O)_2$ was the intermediate, which on complete dehydration changed to $Zn_3V_2O_8$. This photocatalyst was used for the waste water treatment, under UV-light [42].

Pei et al. synthesized zinc vanadate nanorods via hydrothermal method. Precursors included zinc acetate and sodium vanadate. Zinc vanadate showed enhanced photocatalytic degradation of methylene blue. Band-gap of zinc vanadate Nanorods was reported to be 2.76eV, showing greater photocatalytic activity than hybrid zinc vanadate [43].

Mazloom net al. reported zinc vanadate nanostructure for the photocatalytic degradation of methylene blue. Co-precipitation method was used for the synthesis of nanostructures using zinc nitrate tetrahydrate, SDS as surfactant and ethylene diamine as pH stabilizer [44].

Cobalt Vanadate ($Co_3V_2O_8$) as a Photocatalyst

A simple solid state method has been reported for the synthesis of various nanostructures of cobalt vanadate such as $Co_3V_2O_8$, CoV_2O_6 and $Co_2V_2O_7$. Schiff base is used to prevent agglomeration. The as-synthesized nanostructures have been tested for the photocatalytic degradation of different azo dye and the maximum degradation was observed by orthorhombic $Co_3V_2O_8$ nanoparticles [45]. Bhuiyan et al. synthesized highly crystalline nanostructures of cobalt vanadate via solid-state reaction technique. The synthesis was carried out at high temperature and the sample obtained was calcined two times, at 700^oC and 750^oC. Structural properties confirmed the synthesis of highly pure CoV_2O_6. Electrochemical properties of the material for further battery applications were studied [85].

Polymers used as a Photocatalyst

A few of the organic as well as inorganic polymers along with metal oxide nanoparticles have been reported for the photocatalytic degradation of toxic azo dyes. Currently, g-C_3N_4 is an extensively used organic polymer for photocatalytic applications. Zhang et al. reported a ZnO layered hydroxide @ graphitic carbon nitride nanocomposite, synthesized by co-precipitation method. Using ZnO-LDH@g-C_3N_4, 90% of MB was degraded after five cycles under UV-Vis irradiation. Such a high efficiency was attributed to efficient separation of photogenerated charge carriers [46].

Zheng et al. synthesized sulphur doped g-C_3N_4 microrods via thermal polymerization. Sulphur doped microporous g-C_3N_4 showed higher photocatalytic degradation of Rh-B, as compared to bulk g-C_3N_4. Increase in pyrolysis temperature resulted in an increase in the surface area, enhanced electron/hole separation and strong visible light absorption of the photocatalyst [47].

Pawar et al. used a facile chemical method and hybridized reduced graphene oxide and CdS nanoparticles with graphitic carbon nitride. Synthesis and purity of the photocatalyst was confirmed by FTIR spectroscopy and XPS analysis. Larger surface area i.e. 70.42m^2g^{-1} resulted in rapid adsorption of dye over the surface of the photocatalyst. The composite showed high photocatalytic activity as compared to bare g-C_3N_4 because of a decrease in charge recombination and enhanced absorption under visible light. High efficiency for the photodegradation of Congo red and Rhodamine B dyes was obtained. This material can prove beneficial for the degradation of other environmental pollutants as well [86].

1.4 Factors for Improving the Photocatalytic Efficiency

Inorganic semiconductor based photocatalytic materials are proving to be efficient for dye degradation and removal of organic pollutants from the environment, by utilizing solar energy. Fabrication of photocatalysts is carried out in order to overcome the low efficiencies of photoconversion. The features required to be modified for better photocatalytic applications include separation of photogenerated charge carriers, increase in surface area, enhanced visible

light absorption Different strategies that can be used to enhance the activity of photocatalysts are discussed below.

1.4.1 Band-Structure Engineering

Band positions of the semiconductor photocatalytic material can be adjusted through band-structure engineering. This helps in efficient utilization of solar energy, which further improves the efficiency of the material for dye degradation. Band gap engineering can be carried out in the following different ways.

1.4.1.1 Quantum Confinement Effect

Quantum confined semiconductor material tends to have high photostability, long excitation lifetime, larger extinction coefficient and above all, they use a single photon to generate multiple electrons. As a result of the previously mentioned parameters, quantumly confined nanomaterial use the solar energy more efficiently, in order to carry out the dye degradation. High yields of fuel i.e., CH_3OH and CH_4 over TiO_2 nanoparticles have been reported with a decrease in particle size. Particles size was controlled as a result of competing effects of charge-carrier dynamics, light absorption efficiency and specific surface area [48]. Zhang et al. reported a nanocomposite of graphene oxide with yttrium and it had a nanoflake structure. GO acted as an electron conductor in Y_2O_3, hence resulted in an increase in the photocurrent density. This material showed high photocatalytic degradation of methylene blue [49]. Luca et al. carried out the photodegradation of methylene blue using quantum confined titanosilicate semiconductor [50].
Posa along with fellow scientists synthesized graphene oxide-TiO_2 nanocomposite, particles had an average size of 3-6nm and showed high efficiency in photocatalytic degradation of Rh-B dye [51].

1.4.1.2 Doped Semiconductors

Efficiency of a photocatalyst can be improved by doping it with a semiconductor or a noble metal. Most of the metal oxide semiconductors have a band gap around 3 eV, which makes them less efficient materials under visible light. Doping of the semiconductor is carried out in order to lower the band gap, thus making the material efficient under visible light as well. Anions like C and N can be used as dopants, the partial oxygen from metal oxides is replaced which in turn

raises the valence band maxima. Pipi et al. reported N-doped mesoporous TiO_2 with Ag, for the visible-light photodegradation of RNO dye. Doping of nitrogen resulted in lowering of band gap [52]. Thota et al. reported the successful doping of Nitrogen and manganese into titania matrix and studied the visible light degradation of methyl red. Doping caused a decrease in band-gap, as nitrogen doping enhanced visible light response and quantum yield, whereas manganese doping inhibited recombination by trapping the electrons [53].

Doping of cations significantly influence the rate of recombination and interfacial electron-transfer rate. To increase the efficiency of the UV active semiconductor photocatalysts, cationic doping into the lattice of the material is carried out. Cationic doping increases the recombination centers by generating delocalized d-states. Photodegradation of organic dyes has been reported using nickel and copper doped ZnS. Doping results in accelerating the migration rate of electrons and holes to the surface of the nanoparticles, thus resulting in an increase in the efficiency of the photocatalyst [54]. Xu et al. observed the photocatalytic degradation of methyl orange using Co-doped ZnO nanoparticles. Absorption edge shifted towards the longer wavelength, and hence photocatalytic efficiency increased [55]. Hence, a dopant causes a change in the charge transfer properties.

1.4.1.3 Solid Solutions

Solid solutions show higher efficiency as compared to the conventional single component solid solutions. Wu et al. reported solid solution of $(GaN)_{1-x}(ZnO)_x$ with a tunable band-gap (2.38-2.76ev). It showed high photocatalytic degradation rate of environmental pollutants. Solid solution resulted in lower lattice deformation and increased redox potential, proving extremely efficient for pollutant degradation [56].

1.4.1.4 Formation of Heterostructure

Improved photocatalytic properties and efficient charge transfer can be carried out by the formation of heterostructure. Semiconductor heterostructure (Type II) prevents recombination by transferring the electrons from higher to lower conduction band and holes from the lower valence band to higher band. Metal semiconductor heterostructure are leading materials used for the separation of electrons and holes. Low band-gap semiconductor couples with Au absorb light in visible region. Here, the delocalization of electrons occur as a result of interaction between the

plasmonic state of gold and excited state of semiconductor. These nano heterostructure are proving to be efficient in photocatalytic dye degradation, water splitting etc. [57]. Nguyen et al . synthesized $ZnFe_2O_4$–TiO_2 photocatalyst having a particle size of 8-9nm, resulting in a decrease in electron hole recombination, Schottkey barrier formed which increased the photodegradation of Rh-B and methyl red [58]. Min et al. synthesized visible light active $BiVO_4/TiO_2$ nanocomposite, exhibiting enhanced photocatalytic activity. These heterostructures exhibited a charge transfer from $BiVO_4$ to TiO_2, visible light response of TiO_2 increased because of grafted vanadate and hence, photodegradation rate of dye enhanced. $InVO_4/TiO_2$ nanostructures showed high photocatalytic dye degradation due to gradient charge transfer, which decreased the rate of recombination. These heterostructures resulted in greater photocatalytic degradation of RhB, because of efficient charge separation [59].

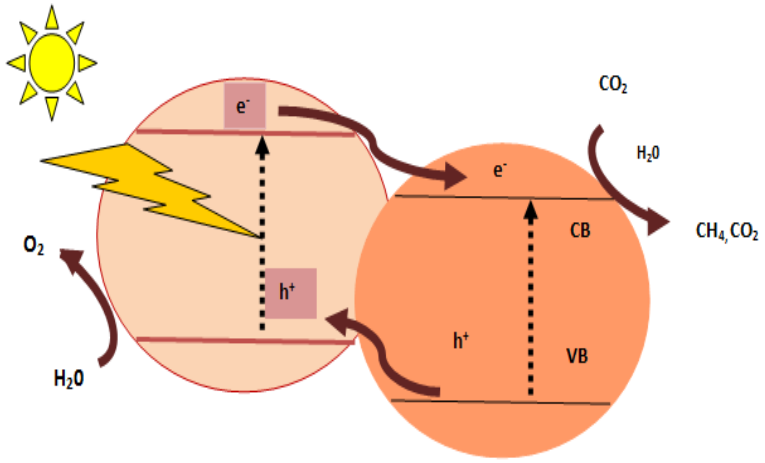

Figure 1.5 Schematic illustration of a semiconductor heterostructure

1.4.1.5 Sensitization of Semiconductors

Most of the metal oxide photocatalysts are efficient under UV light, because of their large band gaps. Only 4% of the solar spectrum comprises of UV light, so in order to improve the photocatalytic efficiency of the material, sensitization can be done. Here, a dye molecule or a narrow band gap material is sensitized with the wider band gap material, in order to make the material visible light active. Photogenerated electrons are transferred from the sensitizer (low band-gap material) to the conduction band of semiconductor (high band-gap material). Most efficient UV light semiconductor includes TiO_2 as it has a wide band gap. CdS, PbS, CdSe are

the narrow band gap semiconductors that can be sensitized with TiO_2. Makama. A. B. reported the synthesis of CdS/TiO_2 nanocomposite for the degradation of methylene blue under visible light. Sensitization resulted in low recombination rate of photogenerated charge carriers [60]. g-C_3N_4/TiO_2 nanocomposites have been used for photocatalytic degradation of rhodamine blue. Optimal concentration of g-C_3N_4 resulted in an increase in lifetime of excited electrons from 2.65 to 10.20 ns, showing efficient charge separation [61].

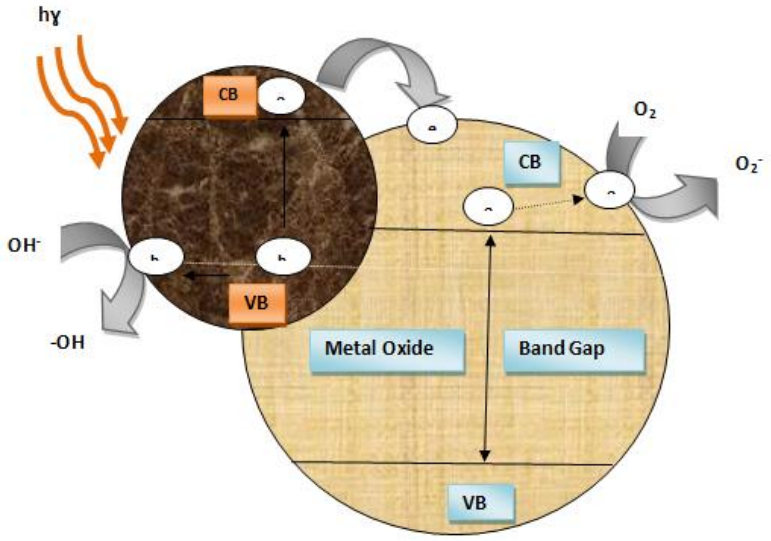

Figure 1.6 Schematic illustration of a wide band gap semiconductor sensitized by small band-gap semiconductor

1.4.2 Nanostructuralization

Single crystal nanomaterials e.g., nanobelts, nanotubes, nanowires etc., show enhanced photocatalytic properties because of the absence of surface defects and grain boundaries. In polycrystalline materials, these surface defects are responsible for increased recombination of photogenerated charge carriers. One dimensional nanomaterials provide efficient charge separation as they possess a direct path for the transport of charges. Semiconductor based materials have been used extensively for the photocatalytic dye degradation. Crystal quality has an inverse relation with the crystal structure defects. Greater the defects in the crystal structure, greater are the chances of recombination, hence lower would be the photocatalytic efficiency. Size of the photocatalyst also affects the photocatalytic activity. Smaller the size of particles, greater would be the surface area and greater would be the number of sites present on the surface

for photolytic reactions [62]. Feng et al. synthesized one-dimensional TiO_2 nanostructures, which included nanotubes, nanobelts and nanowires. Photocatalyst showed excellent photocatalytic dye degradation as a result of increased surface area, suppression of electron-hole recombination and lowering of band-gap [63]. Souderi et al. synthesized TiO_2 thin film having larger exposed surface area. Titania film along with Si nanostructures exhibited 12 times higher photodegradation rate of methyl orange and methylene blue, as compared to flat TiO_2 film [64]. Nalini et al. carried out the UV-light irradiation of bulk Bi_4NbO_8Cl and nano Bi_4NbO_8Cl and measured there photocatalytic activity. Faster degradation of Congo red was carried out by nano Bi_4NbO_8Cl [65].

1.4.3 Engineering the Surface Oxygen vacancies

Photocatalytic efficiency of a material is strongly dependent on its chemical and optoelectronic properties. One of the intrinsic defects, in metal oxide semiconductors, is the oxygen vacancy. This vacancy provides reactive sites on the surface of photocatalytic material, which help in tuning the chemical and electronic properties of the material. CO_2 reduction can be done by tuning these properties. CO_2 molecules get adsorbed into these oxygen vacancies, because of the lowered reactive barrier. Wang et al. reported the significance of oxygen vacancies on the surface of ZnO nanoparticles. These vacancies shifted the absorption edge to longer wavelength, narrowed the band-gap and increased the absorption of ZnO under visible light. Hence, ZnO nanoparticles, with oxygen vacancies resulted in higher photodegradation rate of the environmental pollutants [66]. Indium doped CeO_2 nanocrystals exhibited 40% higher photodegradation rate of dyes, as compared to un-doped indium. Variation in oxygen vacancies attributed towards increased efficiency. More oxygen vacancies were generated as a result of indium doping, decreasing the recombination rate [67].

1.4.4 Development of Porous Structures with Large Surface Area

Large surface area is responsible for the greater adsorption of the reactants (i.e., CO_2, H_2O). Surface area is directly proportional to the number of active sites present on the surface of the material. Three major categories of nanomaterials on the basis of pore size include:

- Microporous material (< 2nm)
- Mesoporous material (2-50nm)
- Macroporous material (>50nm)

Among these, mesoporous materials are most efficient towards photocatalytic dye degradation. Efficient charge separation and transfer of charge carriers occurs because of the high surface area and high degree of crystallinity of the mesoporous photocatalysts. Porous MoO_3 nanoplates have been reported to exhibit excellent photocatalytic performance under visible light, against the degradation of methylene blue. High photocatalytic efficiency was obtained due to efficient charge transport, suppression of recombination and increased surface area [68].

1.4.5 Co-catalysts Assisted Semiconductor-Based Photocatalysts

Co-catalysts play a significant role in increasing the catalytic performance under visible light. Formation of Schottkey barrier between co-catalyst and the semi-conductor enhances the charge separation of the photogenerated electrons and holes, which reduces the recombination of charge carriers. Different metal nanoparticles that can be used as co-catalysts include Au, Ag, Pt, Pd, Cu etc. Electron transfer between the semiconductor material and co-catalysts is easy, as the Fermi level of these co-catalysts lies just beneath the conduction band of the photocatalyst. 19.3% Thallium doped $BiVO_4$ showed enhanced photocatalytic activity as compared to pristine $BiVO_4$ nanoparticles, because of the decrease in recombination rate as a result of the formation of Schottky barrier between the co-catalyst and semiconductor photocatalyst [69].

Xue. J reported plasmonic Au/Pt/g-C_3N_4 photocatalyst for dye degradation under visible light. Electron-hole separation of g-C_3N_4 was facilitated by the plasmonic resonance effect of Au, and Pt nanoparticles acting as an electron sink [70].

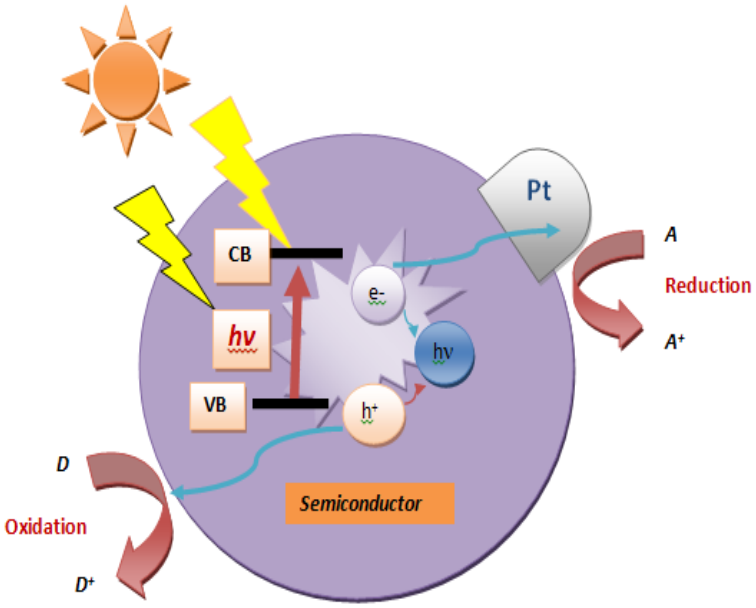

Figure 1.7 Schematic illustration of a co-catalyst assisted semiconductor-based

1.5 Synthesis of Nanomaterial

Material at nanoscale shows enhanced properties (i.e. electrical, mechanical, magnetic, photocatalytic etc.). This is because of the fact that, as the particle size decreases, surface area of the material increases which in turn increases the efficiency of the material. Physical and chemical properties of a material can be modified by using fine synthesis techniques. Top-down and Bottom-up are the two approaches used for the synthesis of nanomaterials.

1.5.1 Top-Down Approach

It involves the successive breakdown of bulk material to get nano sized material. A bulk material is taken and is then modified to get the desired size. Renowned top-down approaches include mechanical milling, lithography etc.

Top-down approach i.e. moderate disintegration exfoliation has been used to synthesize the g-C_3N_4 nano sheets from bulk g-C_3N_4. Dilute H_2SO_4 has been used as an efficient knife for the disintegration and exfoliation of g-C_3N_4. 2D nanosheets with seven atom possessed high surface

area i.e. $80 m^2 g^{-1}$, thereby showed greater charge transfer and separation. Nanosheets of g-C_3N_4 have shown greater photocatalytic degradation of environmental pollutants [71]. Luo et al. reported the synthesis of monoclinic $BiVO_4$ nanoparticles by ball milling method. Annealing of the sample resulted in the elimination of induced defects and thereby enhanced the reactivity. Morphology, crystalline structure and visible light absorption studies were carried out, using different characterization techniques. $BiVO_4$ nanoparticles showed high efficiency towards the photocatalytic degradation of Congo red and Rhodamine B [72].

1.5.2 Bottom-Up Approach

Bottom-up approach refers to the stepwise building of nanomaterials. Firstly, a molecular precursor is decomposed and atoms and molecules are generated. Secondly, nucleation of the atoms and the molecular segments occur and nanomaterial forms. On the basis of phase, bottom-up approach can be classified into the following types.

- Liquid phase synthesis
- Gas phase synthesis

Pyrolysis, Inert gas condensation etc. falls under gas phase fabrication. Liquid phase fabrication is the most commonly used technique and it can be classified into hydrothermal, microemulsion, sol-gel processing, co-precipiatation method, sonochemical method etc. Co-precipitation method will be discussed in detail because the nanocomposite has been synthesized by using this method.

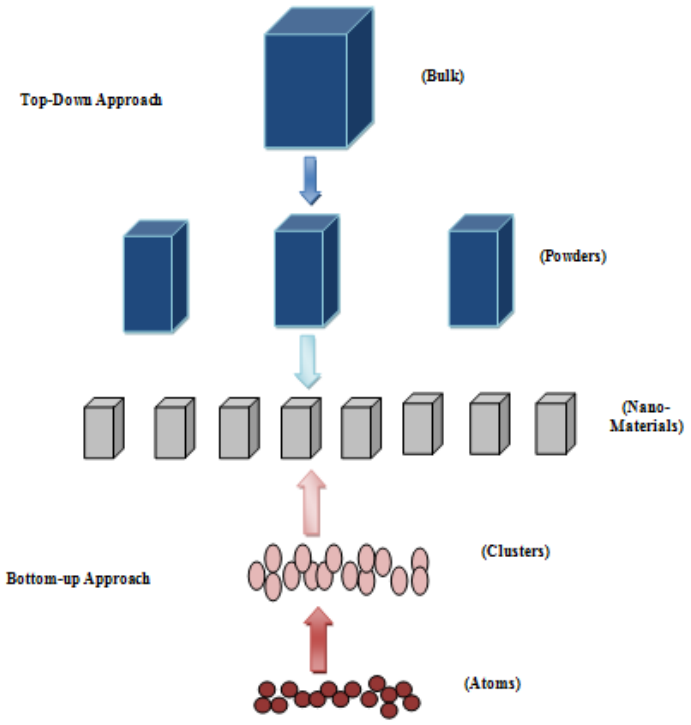

Figure 1.8 Schematic illustration of top-down and bottom-up approach

1.5.2.1 Sol-gel Method

Sol-gel method comprises of two basic steps i.e. hydrolysis followed by condensation. A stable sol forms, then gelation occurs as a result of condensation and finally the gel ages into a solid mass. A semi-rigid mass that forms as a result of evaporation of solvent is the ‘gel, whereas suspension of solute particles within the solvent is the ‘sol’. Hydroxyl groups that are present are removed at high temperatures in order to get a stable gel. The parameters including pH, reaction temperature and reaction time control the size of the particles formed.

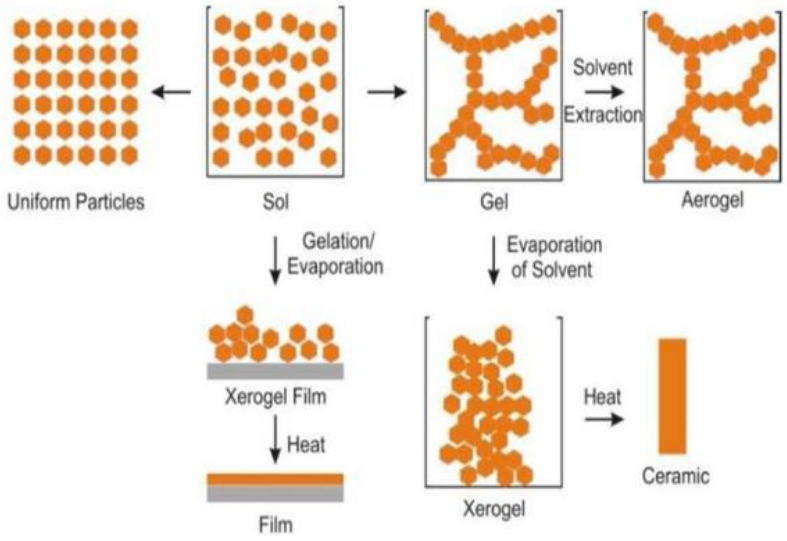

Figure 1.9 Sol-gel synthesis of nanoparticles

Pookmanee et al. synthesized monoclinic $BiVO_4$ by sol-gel method. Bismuth nitrate and ammonium vanadate were used as precursors for the synthesis of $BiVO_4$. Single phase product was obtained after calcining at 400-600^oC. Temperature influenced the morphology of the $BiVO_4$ nanoparticles. Less agglomeration was observed at low temperature [87]. Vanadium doped zinc oxide nanoparticles synthesized via sol-gel method have been reported for the photodegradation of environmental pollutants. Supercritical drying of ethyl alcohol resulted in slow release of water of hydrolysis. Sample was calcined at 500^oC and the average particle size was found out to be 25nm. Upto74% degradation of organic pollutants was carried out by vanadium doped zinc oxide nanoparticles [88].

Li et.al reported the synthesis of hybrid g-C_3N_4-TiO_2 photocatalyst by using sol-gel method. Composites had varying concentrations of g-C_3N_4. Different characterization techniques have been used to study the interface properties and microstructure of the photocatalyst. Heterojunction formed between TiO_2 and g-C_3N_4 increased the photodegradation efficiency of hybrid g-C_3N_4-TiO_2. Photodegradation of methylene blue was carried out and the hybrid exhibited 3.5 times greater efficiency as compared to bare g-C_3N_4. A very low photo-activity loss was observed even after 5cycles [89].

1.5.2.2 Microemulsion Method

Two immiscible liquids forming a stable isotropic dispersion is known as microemulsion. For example, water and oil, interfacial films or surface active molecules help in the stabilization of both liquids. Microemulsions can be normal (i.e., oil-in-water) and reverse (i.e., water-in-oil). Surfactant is added into the reaction mixture. The hydrophilic head of the surfactant is towards the water and hydrophobic tail towards the oil. Particles with controlled size are synthesized by this technique.

Microemulsion method results in the synthesis of particles having large interfacial area, ultra-low interfacial tension, high solubility and thermodynamic stability. Nanoparticles synthesized using microemulsion technique find vast applications as ceramic materials, catalysts, in drug delivery etc. Different parameters that can be controlled include geometry, particle size, morphology, surface area and homogeneity. Besides this, microemulsion method helps in controlling the grain size and morphology at the same time. Different semiconductor based nanomaterials (ZnO, ZnS etc.) for degradation of environmental pollutants have been synthesized by using microemulsion technique [90].

1.5.2.3 Hydrothermal Method

The word "hydro" means water and "thermal" means heats. In case of any other solvent than water, this method is known as Solvothermal method. This method involves the formation of single crystal at high temperature and high pressure. Hydrothermal method can be defined as a heterogeneous chemical reaction in the presence of an aqueous solvent above atm. temperature and atm. pressure. Morphology, crystallinity and particle size of the nanoparticles greatly depends on the temperature and pressure of the reaction mixture. High purity product with uniform size distribution is achieved via hydrothermal synthesis, and it is a commonly used route for the synthesis of metals and metal oxide nanoparticles. It consists of a Teflon body, enclosed in a steel chamber.

Hydrothermally synthesized g-C_3N_4/$InVO_4$ nanocomposite and g-C_3N_4-$CdWO_4$ nanocomposite have been reported for efficiently degrading the toxic dyes i.e. methyl orange etc. Heterojunction type photocatalyst synthesized by in-situ growth of $InVO_4$ over the surface of g-C_3N_4 has been reported. Intimate interface inhibited the charge recombination and promoted the charge transfer, as a result of which the photocatalytic activity was improved. Effective charge separation and

greater reducing power increased the H_2 evolution from water splitting. Bare g-C_3N_4 and $InVO_4$ showed less photocatalytic activity as compared to the composite [91].

1.5.2.4 Sonochemical Method

It is an efficient chemical method used for the synthesis and coating of nanoparticles. This method leads to the formation of acoustic cavitation in liquids by using the ultrasound waves. Acoustic cavitation refers to the formation, growth and implosive collapse of bubbles. In this method, the solution is irradiated by using high intensity ultrasound waves, as a result of which chemical reactions occur within the bubble. After it, the bubble collapses, atoms diffuse into the liquid phase, nucleation occurs and nanomaterial forms. Hence, sonochemical method involves acoustic cavitation, growth followed by rapid collapse of bubbles which provides energy for the chemical reactions, and this is known as sonochemistry. Extraordinary conditions i.e. 20,000 K temperature and several thousand bars pressure can be achieved in sonochemical method [92, 93].

1.5.2.5 Co-precipitation Method

Co-precipitation method is a commonly used method for the synthesis of oxide ceramics. The precipitates formed as a result of co-precipitation method comprises more than one insoluble species, which is then separated from the solution. Nucleation is the major step involved in this process. Size and morphology of nanoparticle is affected by Ostwald ripening and agglomeration. Most commonly used precursors include inorganic salts (Sulphate, chloride and nitrate), dissolved in water or any other solvent and a homogeneous solution forms. Precursor concentration, temperature, pH influence the crystal growth and aggregation. Solid mass is obtained as after precipitation, which is then washed and dried. Agglomeration in the final product is dependent on the washing and drying procedures. Co-precipitation method has a number of advantages.

- Solutions formed is homogeneous
- Reaction proceeds at a relatively low temperature
- Uniform particle size
- Low cost

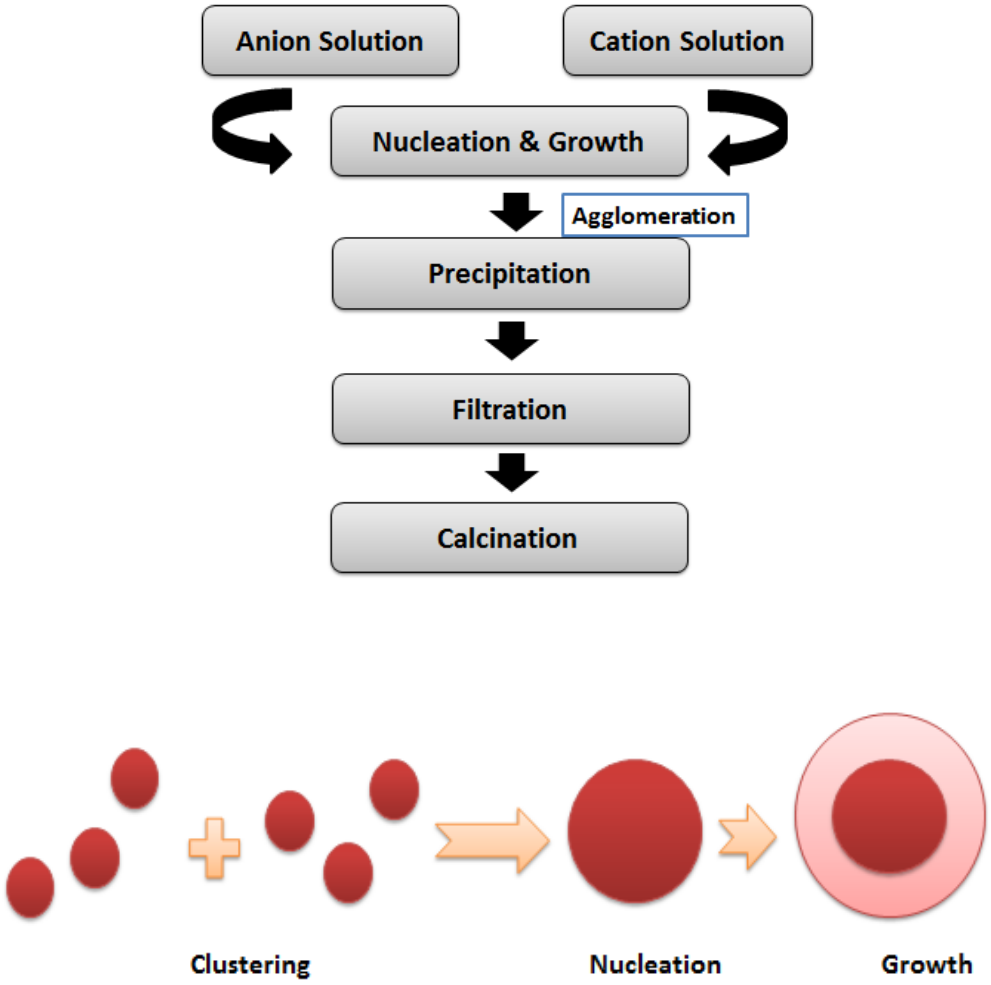

Figure 1.10 Schematic representation of Co-precipitation method

$Zn_3V_2O_8$ nanostructures synthesized by co-precipitation method have been reported using anionic sodium dodecyl Sulphate as a surfactant. Effect of different parameters, such as reaction temp, time, pH were studied. Ghorbani et al reported the synthesis of ZnO nano particles by co-precipitation method. Zinc nitrate solution was stirred with constant addition of KOH at room temperature. Stirring resulted in the formation of white precipitates, which were centrifuged, washed with water and ethanol and annealed at 500^{o}C [94]. Chang Chun Chen also prepared ZnO nanoparticle by direct precipitation method by using zinc nitrate and ammonium carbonate as precursors. A white suspension was formed which was then precipitated, centrifuged and washed. Particles had an average crystallite size of 17nm [95].

1.6 Scope of Work

Energy and environmental crisis are the two major emerging problems of the current world. Various factors are contributing largely towards environmental contamination, so the removal of toxic environmental pollutants is of concern. As these toxic contaminants are affecting human, aquatic life and atmosphere equally. Efficient measures are required to be taken in order to control the level of environmental pollution. Photocatalysis is a promising approach towards the environmental remediation. Different cost effective photocatalytic materials are used excessively for the removal of organic contaminants. This method utilizes an infinite energy source i.e solar energy, hence making it an economical approach.

Vanadates are emerging as efficient photocatalysts because of their cost effectiveness, easy availability and greater efficiency towards the removal of toxic environmental pollutants. Besides this, organic polymers are also proving to be highly efficient photocatalysts. Most commonly used organic polymer for photocatalytic applications is g-C_3N_4. It possesses easy synthesis approach and is cost effective. Different factors need to be kept in account in order to increase the efficiency of a photocatalytic system. The approach used in my work is the formation of heterostructures, in order to increase the charge separation so as to carry out the surface reactions effectively.

Here, we have focused on the synthesis of $Co_3V_2O_8/Zn_3V_2O_8$ and $Co_3V_2O_8$/g-C_3N_4 nanocomposites. Co-precipitation is an easy and economical synthesis approach used to synthesize $Co_3V_2O_8/Zn_3V_2O_8$ nanocomposites. Physical method is used for the synthesis of $Co_3V_2O_8$/g-C_3N_4 photocatalysts. Both these photocatalyst heterostructures are efficient photocatalytic systems.

References

1) S. Shafiee and E. Topal, *Energy Policy*, **2009**, 37, 189

2) S. Reddy and J. P Painuly, *Renewable Energy*, **2004**, 29, 1447

3) J. Twiddle and T. Weir, *Renewable Energy Sources*, 3rd edition, **2015**

4) R. York, *Nature and Climate Change*, **2012**, 2, 443

5) A. V. Bridgewater, *Chemical Engineering Journal*, **2003**, 91, 87-102

6) N. L. Panwar, S. C. Kaushik and S. Kothari, *Renewable and Sustainable Energy Reviews*, **2011**, 15, 1513-1524

7) T.B. Johansson. H. Kelly, A. K. N. Reddy and R.H. Williams, *Renewable Energy Sources for Fuel and Electricity*, **1993**

8) D. Bahnemann, *Solar Energy*, **2004**, 77, 445-459

9) A. Wellburn, *Air Pollution and Acid Rain:* The Biological Impact. New York: Wiley, **1988**

10) F. Rehman, *Journal of Textile Science and Engineering*, **2016**, 6, 242.

11) A. K. Mishra and S. Ramaprabhu, *Chemical Engineering Journal*, **2010**,162, 1026-1034.

12) V. Karthik, K. Saravana, P. Bharathi, V. Dharanya and C. Meiaraj, 2014, *Journal of Chemical and Pharmaceutical Sciences*, **2007**, 31, 301-307

13) V. S. Houk, *Mutation Research*, **1992**, 277, 91-138.

14) A. B. D. Santos, F. J. Cervantes, J.B. Lire, *Bioresource Technology*, **2007**, 98, 2369-2385.

15) T. Robinson, G. McMullan and R. Merchant, *Bioresource Technology*, **2001**, 77, 247-255.

16) M. Kashefi and F. Bahrami, *Bulletin of Georgian National Academy of Sciences*, **2014**, 8.

17) A. Kumar, P. Chaudhary and P. Verma, *Global Journal of Environmental Research*, **2011**, 5, 46-52

18) K. Y. Show and D. J. Lee, *Biological Treatment of Industrial Effluents*, **2017**, 205-230.

19) Frank P. van der Zee and S. Villaverde, *Water Research*, **2005**, 39, 1425-1440.

20) Y. J. Chan, M. F. Chong, C. L. Law and D. G. Hassell, *Chemical Engineering Journal*, **2009**, 155, 1-18

21) A. R. Baghr, N. M. Mahmoodi and F. M. Menger, *Desalination*, **2010**, 260, 34-38.

22) S. Liakou, S. Pavlou and G. Lyberatos, *Water Science and Technology*, **1997**, 141, 279-286.

23) O. Karahan, H. Dulkadiroglu, I. Kabdasli, S. Sozen, F. G. Babuna and D. Orhon, *Environmental Technology*, **2002**, 23, 1325-1336.

24) N. Serpone, E. Pelizzetti, *Photocatalysis: Fundamentals and Applications*, Wiley, New York, **1989**.

25) S. H. S. Chan, T. Y. Wu, J. C. Juan and C. Y. The, *Journal of Chemical Technology and Biotechnology*, **2011**, 86, 1130-1158.

26) S. Malato, J. Blanco, A. Vidal and C. Richter, *Applied Catalysis B: Environmental*, **2002**, 37, 1-15.

27) P. Ciesla, P. Kocot, P. Mytych and Z. Staticka, *Journal of Molecular Catalysis A: Chemical*, **2004**, 224, 17-33

28) J. M. Herrmann, *Catalysis today*, **1999**, 53, 115-129.

29) M. I. Litter, *Applied Catalysis B: Environmental*, **1999**, 23, 89-114

30) S.G. Kumar and L.G. Devi, *The Journal of Physical Chemistry A*, **2011**, 46, 13211-13241

31) K. Kabra, R. Chaudhary and L. S. Rameshwar, *Industrial & Engineering Chemistry Research*, **2004**,43, 7683-7696.

32) C. Cheng, W. Ma and J. Zhao, *Chemical Society Reviews*, **2010**, 39, 4206-4219.

33) J. S. Lee, J. Jhang, *Journal of Industrial and Engineering Chemistry*, **2014**, 20, 363-371

34) M. M. Khan, S. F. Adil, and A. AL-Mayouf, *Journal of Saudi Chemical Society*, **2015**, 19, 462-464

35) A. L. Linsebigler, G. Q. Lu and J. T. Yates, *Chemical Reviews*, **1995**, 95, 735-758

36) D. L. Greenaway and G. Harbeke, *Optical Properties and Band Structure of Semiconductors: International Series of Monographs in the Science of The Solid State*, **2015**, 1, Elsevier.

37) A. Alshammari, A. Bagabas and M. Assulami, *Arabian Journal of Chemistry*, **2014**, 1, 13-16

38) M. Amini and M. Ashrafi, *Nanochemistry Research*, **2016**, 1, 79-86

39) M. M. Rashad, A. A. Ismail, I. Osama, I. A. Ibrahim and A. T. Kandil, *Arabian Journal of Chemistry*, **2014**, 7, 71-77

40) M. Yan, Y. Wu, Y. Yan, X. Yan, F. Zhu, Y. Hua and W. Shi, *Sustainable Chemistry and Engineering*, **2016**, 4, 757-766

41) G. Odling and N. Robertson, *ChemPhysChem*, **2016**, 17, 2872-2880

42) C. Mondal, M. Ganguly, A. K. Sinha, J. Pal, R. Sahoo and T. Pal, *Crystal Engineering Communication*, **2013**, 34

43) L. Z. Pei, N. Lin, T. Wei, H. D. Liu and H. Y. Yu, *Journal of Alloys and Compounds*, **2015**, 631, 90-98.

44) F. Mazloom, M. M. Arani, M. G. Arani and M. S. Niasari, *Journal of Molecular Liquids*, **2016**, 214, 46-53.

45) M. G. Arani, M. M. Arani and M.S. Niasari, *Journal of Molecular Catalysis A: Chemical*, **2016**, 425, 31-42

46) L. Zhang, L. Li, X. Sun, P. Liu, D. Yang and X. Zhao, *Materials*, **2016**, 9, 1-16

47) Y. Zheng, Z. Yu, F. Lin, F. Guo, K. A. Alamry, L. A. Talib, A. M. Asiri and X. Wang, *Molecules*, **2017**, 22, 572

48) K. Koci, L. Obalova, L. Matejova, D. Placha, Z. Lacny, J. Jirkovsky and O. Solcova, *Applied Catalysis B,* **2009**, *89,* 494-498

49) Y. Zhang, S. Yuan, H. Wang and C. He, *Journal of Materials Chemistry A*, **2014**, 21

50) V. Luca, M. Osborne, D. Sizgek, C. Griffith and P. Z. Arauju, *Chemistry of Materials*, **2006**, 18, 6132-6138

51) V. R. Posa, V. Annavram, J. R. Koduru, P. Bobbala, V. Madhavi and A. R. Somala, *Journal of Experimental Nanoscience*, **2016**, 11, 722-736

52) A. Pipi, G. Byzynski and L. Ruotolo, *Journal of Materials Research*, **2017**, 3, 628-638

53) S. Thota, S. R. Tirukkovalluri and S. Bojja, *Journal of Catalysts*, **2014**, 4, 37-42

54) H. M. Pouretedal, A. Norozi, M. H. Keshavarz and A. Semnani, *Journal of Hazardous Materials*, **2009**, 162, 674-681

55) S. Fabbiyola, L. J. Keneddy, U. Aruldoss, M. Bououdina, A. A. Dakhel and J. J. Vijaya, *Powder Technology*, **2015**, 286, 757-765

56) A. Wu, J. Li, B. Liu, W. Yang, Y. Jiang, L. Liu, X. Zhang, C. Xiong and X. Jiang, *Dalton Transcations*, **2017**, 8, 333-339

57) S. K. Dutta, S.K. Mehetor and N. Pradhan, *The Journal of Physical Chemistry Letters*, **2015**, 6, 936-944

58) T. B. Naguyen and R. Doong, *RSC Advances*, **2016**, 105, 66-74

59) Y. Min, K. Zhang, Y. C. Chen and Y. G. Zhang, *Chemical Engineering Journal*, **2011**, 175, 76-83

60) A. B. Makama, A. Salmiaton, E.B. Saion, T.S.Y. Choong and N. Abdullah, *International Journal of Photoenergy*, **2016**, 122, 44-48

61) M. Sharma, S. Vaidya and A. K. Ganguli, *Journal of Photochemistry and Photobiology A: Chemistry*, **2017**, 335, 287-293

62) N. Lubick and K. Betts, *Environmental Science and Technology*, **2008**, 42, 3910

63) T. Feng, G. S. Feng, L. Yan, J. H. Pan, *International Journal of Photoenergy*, **2014**, 132, 66-74

64) V. Scuderi, G. Impellizzeri, L. Romano, M. Scuderi, G. Nicotra, K. Bergum, A. Irrera, B .G. Svensson and V. Privitera, *Nanoscale Research Letters*, **2014**, 9, 458-465

65) S. S. M. Bhat and N. G. Sundaram, *New Journal of Chemistry*, **2015**, 39, 3956-3963

66) J. Wang, Z. Wang, B. Huang, Y. Ma, Y. Liu, X. Qin and X. Ying, *Applied Material and Interfaces*, **2012**, 4, 4024-4030

67) A. Younis, D. Chu, Y. V. Kaneti and S. Li, *Nanoscle*, **2016**, 8, 378-386

68) Y. Liu, P. Feng, Z. Wang, X. Jiao and F. Akhtar, *Scientific Reports*, **2017**, 7

69) A. Malathi, V. Vasanthakumar, P. Arunachalam and M. Jagannathan, *International Journal of Photoenergy*, **2017**, 5, 77-91

70) J. Xue, S. Ma, Y. Zhou, Z. Zhang and M. He, *Applied Materials and Interfaces*, **2015**, 7, 9630-9637

71) A. Wang, C. Wang, L. Fu, W. Wong and Y. Lan, *Nano-Micro Letters*, **2017**, 9, 47-55

72) Q. Luo, L. Zhang, X. Chen, O. K. Tan and K. C. Leong, *RSC Advances*, **2016**, 19, 2006-2018

73) C. B. Ong, A. W. Mohammad, R. Rohani, M. M. Abbad, N. H. H. Hairmon, *Process Safety and Environmental Protection*, **2016**, 104, 549-557

74) S. Erdemoglu, S. K. Aksu, F. Savilkan, B. Izgj, H. Savilkan, F. Frimmel and S. Gucer, *Journal of Hazardous Materials*, **2008**, 155, 469-476

75) M. Yusuf, M. Shabbir and F. Muhammad, *Natural Products and Bioprospecting*, **2017**, 7, 123-145

76) I. Ayadi, Y. Souissi, I. Lassi, F. Peixoto and W. Mnif, *Journal of Developing Drugs*, **2016**, 5, 155-172

77) L. M. Games and R. A. Hites, *Journal of Analytical Chemistry*, **1977**, 49, 1433-1440

78) M. K. Dahri, M. R. R. Kooh and L. B. L. Lim, *Environmental Chemistry*, **2013**, 19, 234-241

79) M. R. Kulkarni, T. Revanth, A. Acharya and P. Bhat, *Resource Efficient Technologies*, **2017**, 3, 71-77

80) N. B. Kurnick, A. E. Mirsky, *Journal of General Physiology*, **1950**, 33, 265-273

81) J. A. Kiernan, *Journal of Biotechnic and Histochemistry*, **2009**, 76, 261-278

82) M. Mirjalili and L. Karimi, *Journal of Chemistry*, **2013**, 43, 58-62

83) P. Ratna and B. S. Padhi, *International Journal of Environmental Sciences*, **2012**, 3, 33-39

84) A. Kudo, H. Kato, I. Tsuji, *Chemistry Letters*, **2004**, 33, 1534-1539.

85) T. H. Bhuiyan, A. Rahman, R. Sultana, R. Mustafa, A. T. Husna and A. R. Sarker, *Journal of Congent Physics*, **2016**, 33, 322-332

86) R. C. Pawar, V. Khare and C. S. Lee, *Journal of Dalton Transactions*, **2014**, 33, 411-425

87) P. Pookemanee, S. Kojinoki and P. Sukon, *Journal of Metals, Materials and Minerals*, **2012**, 22, 49-53

88) J. E. Ghoul, C. Barthou and L. E. Mir, *International Journal of Environmental Sciences*, **2012**, 51, 942-951

89) C. Li, Z. Sun, Y. Xue, G. Yao and S. Zheng, *Advanced Powder Technology*, **2016**, 27, 330-337

90) M. A. Malik, M. Y. Wani and M. A. Hashim, *Arabian Journal of Chemistry*, **2012**, 5, 397-417

91) B. Hu, T. Chen, M. Fan, C. Song, X. Yan and W. Shi, *Journal of Applied Material Interfaces*, **2015**, 33, 247-256

92) K. S. Suslick and D. J. Flannigan, *Annual Review of Physical Chemistry*, **2008**, 59, 659.

93) K. S. Suslick, Science, **1990**, 247, 1439.

94) H. R. Ghorbani, F. P. Mehir H. Pazoki and B. M. Rahmani, *Oriental Journal of Chemistry*, **2015**, 31, 1219-1221.

95) C. C. Chena, B. Yua, P. Liub, J. F. Liua and L. Wanga, *Journal of Ceramic Processing Research*, **2011**, 12, 420-425.

Experimental Details

Abstract

This chapter encompasses the experimental details, chemicals used for the synthesis of photocatalysts, various techniques used for the characterization of synthesized material and the procedure opted for the photocatalytic dye degradation. Synthesis of $Co_3V_2O_8/Zn_3V_2O_8$ chemical composites and $Co_3V_2O_8$/g-C_3N_4 physical composites has been discussed in detail. Photocatalytic degradation of Congo red and its mechanism has been discussed in detail.

2.1 Chemicals

Chemicals used for the synthesis of $Co_3V_2O_8/Zn_3V_2O_8$ nanocomposite and $Co_3V_2O_8$/g-C_3N_4 nanocomposite are of analytical grade and were used without any further purification. Details about the chemicals used have been provided in **Table 2.1**

Table 2.1 Chemicals used for the synthesis of photocatalysts

Chemical	**Molecular Formula**	**%age Purity**	**Supplier**
Cobalt Chloride Hexahydrate	$CoCl_2.6H_20$	99.8	Sigma Aldrich
Zinc Acetate	$Zn(CH_3COO)_2$	99.99	Sigma Aldrich
Sodium Dodecyl Sulphate (SDS)	$C_{12}H_{25}NaO_4S$	98.77	Sigma Aldrich
Ammonium Metavanadate	NH_4VO_3	99	Sigma Aldrich
Ethanol	C_2H_5OH	99	Sigma Aldrich
Sodium Hydroxide	NaOH	99.99	Sigma Aldrich
Melamine	C_3H_6N	99.99	Sigma Aldrich

2.2 Synthesis of $Co_3V_2O_8$ Nanoparticles

$CoCl_2.6H_20$ and NH_4VO_3 with a molar ratio of 3:2 were used to synthesize $Co_3V_2O_8$ nanoparticles, in the presence of SDS surfactant. 30mM $CoCl_2.6H_20$ solution was prepared by dissolving 356.85mg of the salt in 50ml DI water. 0.5 g SDS was added to the salt solution. 20mM NH_4VO_3 i.e., 117mg in 50ml was prepared and added dropwise to the above solution for 2h, under continuous magnetic stirring. Color change from light purple to dark green was observed. NaOH solution was added in order to adjust the pH from 8-9. Finally the mixture was centrifuged at 7000 rpm for 10min, washed with water and ethanol. The sample was dried in vacuum oven for 4h at 60°C and then annealed at 450°C for 2h. Dark green nanoparticles of $Co_3V_2O_8$ were obtained.

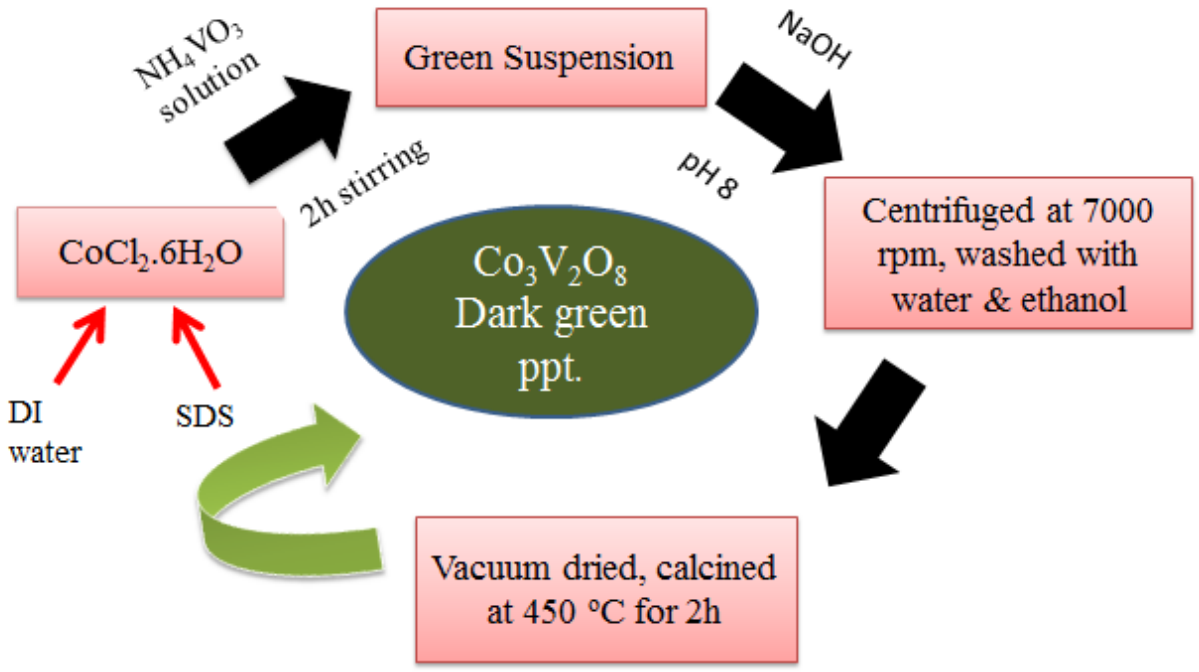

Figure 2.1 Schematic representation of the synthesis of $Co_3V_2O_8$ nanoparticles

2.3 Synthesis of $Zn_3V_2O_8$ Nanoparticles

$Zn_3V_2O_8$ nanoparticles were synthesized using $Zn(CH_3COO)_2$ and NH_4VO_3(3:2), and SDS was used as a surfactant. 275.22mg zinc acetate (30mM) was dissolved in 50ml DI water with simultaneous addition of 0.5g SDS to this solution. 117mg NH_4VO_3 was dissolved in 50ml DI water (20mM). Dropwise addition of ammonium metavanadate solution into the previously prepared solution was carried out for 2h. Gradually, the color of the solution changed from white to yellow. A few drops of NaOH solution were added in order to adjust the pH between 8 and 9. The mixture was centrifuged at 7000rpm for 10min, and then washed with water and ethanol. Precipitates were vacuum dried at 60°C for 4h. Finally the powdered ppt. was subjected to calcination at 450°C for 2h. White precipitates of $Zn_3V_2O_8$ were obtained.

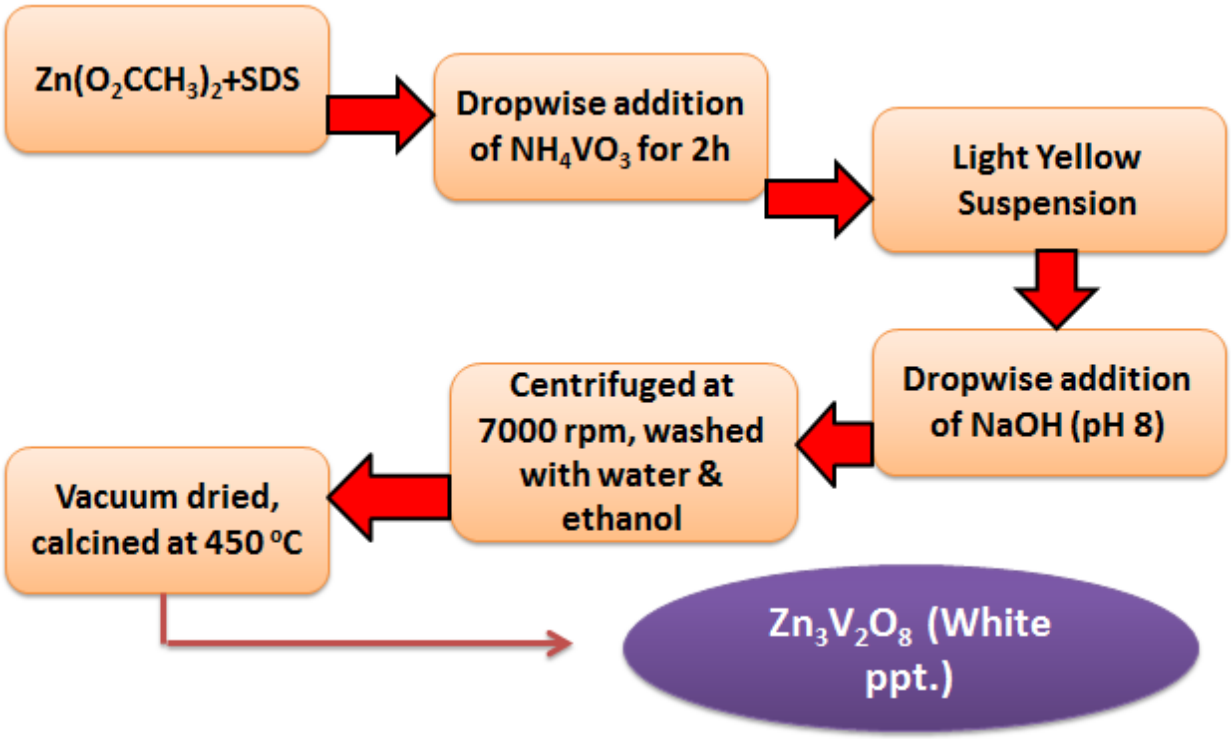

Figure 2.2 Schematic representation of the synthesis of $Zn_3V_2O_8$ nanoparticles

2.4 Synthesis of g-C_3N_4

Precursor used for the synthesis of g-C_3N_4 includes melamine. 5g melamine was placed in an aluminum combustion boat. The sample was heated at 550°C for 2 hours, with a heating rate of 3°C/min. Yellow agglomerates of g-C_3N_4 were obtained, which were than ground properly.

2.5 Synthesis of $Co_3V_2O_8/Zn_3V_2O_8$ Nanocomposite

Chemical composites of $Co_3V_2O_8/Zn_3V_2O_8$ were prepared by varying the molar ratios and keeping the total molarity 30mM. In a typical procedure, 118.8mg of $CoCl_2.6H_2O$ (20mM) was dissolved in 25ml of DI water. 45.87mg of Zinc Acetate (10mM) solution in 25ml DI water was added to the previously prepared solution. 0.5g of Sodium Dodecyl Sulphate (SDS) was added as a surfactant. 117mg NH_3VO_4 (20mM) dissolved in 50ml DI water was added dropwise to the previously prepared solution for 2h, under constant magnetic stirring. Color change was observed till the end of the reaction. Finally, NaOH solution was added to shift the pH of the solution to 8. The mixture was centrifuged at 7000rpm for 10min, product dried under vacuum for 4h at 60^{o}C. Finally the sample was calcined at 450^{o}C for 2h. Same procedure was followed to synthesize different composites i.e. $Co_3V_2O_8$= 5mM, 2mM and $Zn_3V_2O_8$= 25mM, 28mM respectively.

Table 2.2 $Co_3V_2O_8/Zn_3V_2O_8$ nanocomposites with different molar concentrations

	$Co_3V_2O_8$	**$Zn_3V_2O_8$**
Composite-1	2omM	10mM
Composite-2	5mM	25Mm
Composite-3	2mM	28Mm

2.6 Synthesis of $Co_3V_2O_8$/g-C_3N_4 Nanocomposite

Physical composites of $Co_3V_2O_8$/g-C_3N_4 were prepared by taking different amounts of as-prepared $Co_3V_2O_8$ and g-C_3N_4, details of which have been shown in **Table 2.3**. Each composite was prepared by grinding precursors for half an hour using agate mortar and pestle.

Table 2.3 Molar ratio and amount of $Co_3V_2O_8$ and g-C_3N_4 in $Co_3V_2O_8$/g-C_3N_4 nanocomposites

Molar Ratio	Amount of $Co_3V_2O_8$ (mg)	Amount of g-C_3N_4 (mg)
$Co_3V_2O_8$/g-C_3N_4 (3:1)	75	25
$Co_3V_2O_8$/g-C_3N_4 (1:1)	50	50
$Co_3V_2O_8$/g-C_3N_4 (1.3)	25	75

2.7 Photocatalytic dye degradation

Photocatalytic activity of $Co_3V_2O_8$/ $Zn_3V_2O_8$ and $Co_3V_2O_8$/g-C_3N_4 nanocomposites was investigated against congo red degradation, by irradiating the samples with UV-Vis light. Degradation of congo red was carried out at room temperature. Source of light used for the degradation of dye was a Xe arc lamp (3000 W). 250ml solution containing 75ppm dye was placed under the source of light, and two blank experiments were carried out. One controlled experiment in the presence of light and dye solution and the other, in the presence of light and catalyst was carried out. In both cases, no spectral loss was observed even after one hour. Then 100mg of each photocatalyst was dispersed in 100ml dye solution separately, and the mixture was irradiated under UV-Vis light. Adsorption-desorption equilibrium was established between the photocatalyst and dye solution. 5ml of the solution from each flask was collected after every 5min for 1h, and the sample was analyzed using UV-Vis spectrophotometer [Shimadzu UV 2550]. The % degradation of congo red, at regular time intervals, was investigated by measuring the change in the concentration of congo red with respect to time.

2.8 Characterization Techniques

The confirmation of the as-synthesized product was carried out by using different characterization techniques. To probe the crystal structure of the product, XRD analysis was carried out. A Rigaku diffractometer with Cu-Kα radiation equipped with graphite monochromator was used for the analysis of crystal structure. XRD patterns were analyzed over a 2θ range i.e. 10^{o}-80^{o} with a time count of 1 second. UV-Visible Spectrophotometer helped in collecting the UV-Vis diffuse reflectance pattern within a wavelength range of 200-800nm. A lambda 750 UV/Visible spectrophotometer with 200-800 wavelength range and was used for collecting UV-visible diffuse reflectance spectra. BaSO4 was used as a reference. SEM was used to determine the morphology of as-synthesized material. EDX gave elemental composition of the product through elemental mapping. . Morphology and composition of as-synthesized product was analyzed by Hitachi S4800 field emission scanning electron microscopy (FESEM) with energy dispersive X-ray spectrometer (EDX) Valence band position and the composition of the photocatalyst was determined by XPS analysis. Instrumentation and working principle of different characterization techniques has been discussed as below:

2.8.1 X-ray Diffraction (XRD)

XRD is a non-destructive analytical technique used for the phase identification of a material. A crystal structure comprises layers or planes etc. When the wavelength of the incident X-rays is similar to the interatomic distance, then angle of reflection becomes equal to the angle of incidence, and this is known as "diffraction". It is described with the help of Bragg's Law i.e. $\mathbf{2dsin\theta = n\lambda}$. Where n= integer, λ = wavelength of X-rays, d= interplanar spacing, θ= diffraction angle. Constructive interference occurs, when Bragg's law is satisfied and the Bragg's reflection is picked up by the detector. Position of the reflected rays provides information about the inter-layer spacing. Peak intensity provides quantitative information about how much of the incident X-ray has contributed to the reflection. Diffraction pattern provides information about the phases present in a sample, crystallinity of material, lattice parameters, crystal structure, cell volume, density etc. [2]. An X-ray spectrum is obtained when the electrons emitted from the cathode, dislodge the electrons from the target material, Kα and Kβ being the most important components of the spectra. Most commonly used target material is Copper, with Cu Kα = 0.54nm

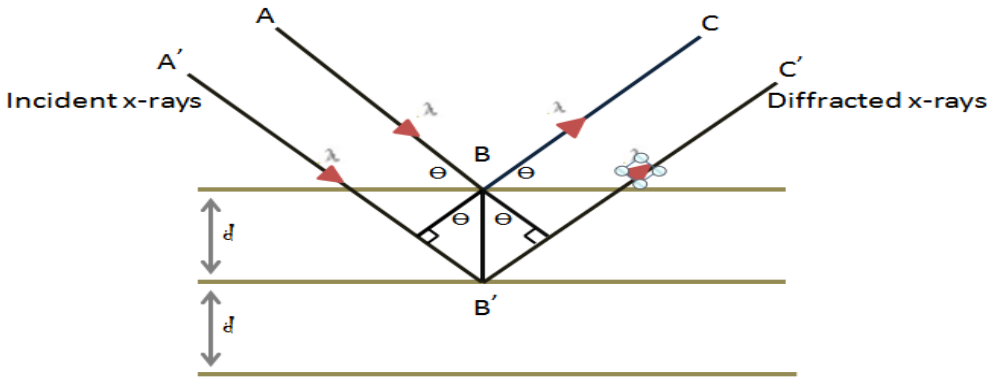

Figure 2.3 Schematic illustration of Bragg's Law

XRD comprises the following components:

- X-ray Source
- Monochromator
- Goniometer (It restricts the wavelength range)
- Sample holder
- Detector

A continuous X-ray beam falls on the crystal. Monochromator filters these X-rays, which then collimate and fall on the sample. Specimen rotates at an angle θ within the path of X-rays. Goniometer is used to rotate the sample. Detector swaps at an angle of 2θ and collects the diffracted X-rays. X-rays diffract and reflect from the layers of the crystal, giving rise to constructive interference. Diffraction pattern is recorded on a photographic film. Beam of reflected X-ray radiation travels larger distance. Constructive interference occurs, when the path difference becomes equal to an integral multiple of wavelength **[1, 7]**.

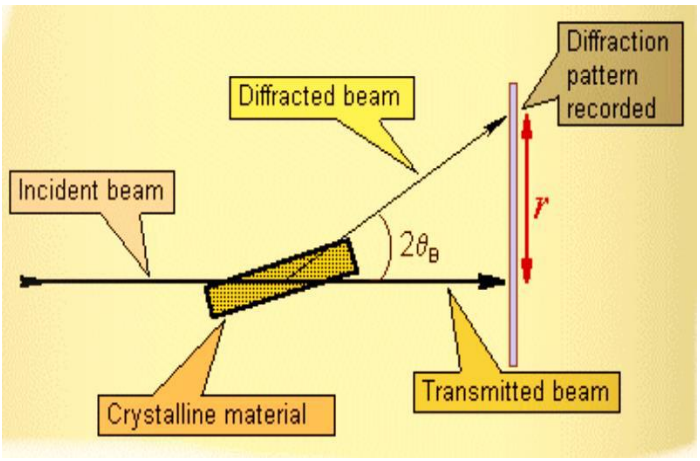

Figure 2.4 Schematic diagram of XRD

XRD finds application in

- crystal structure determination
- determination of grain size, texture, composition of thin film
- phase identification

2.8.2 Fourier Transform Infrared Spectroscopy (FT-IR)

FTIR stands for fourier transform infra–red spectroscopy. It gives information about the chemical bonding present within a material. FTIR is mostly used for the non-destructive analysis of thin films and solid samples. Infrared region ranges from 12800~ 10cm-1 and is divided into three main regions. FTIR spectroscopy basically incorporates the mid infrared region (4000 ~ 200 cm-1), because most of the organic and inorganic ions show absorption in this region. In IR spectroscopy, molecules show characteristic absorption of the infrared radiation, which helps in determining the structure of the molecule.

When the sample is irradiated by IR rays, sample molecules absorb rays of specific wavelength which causes a change in the dipole moment of the molecule. Vibrational energy levels get transferred from ground to excited state, vibrational energy gap gives the frequency of absorption peak. It basically deals with the change in the intensity of IR radiation with respect to wavelength. Intensity of the peaks depends on the change of dipole moment and transitions among the energy levels. An FTIR spectrum is plotted between wavenumber and

absorbance/transmittance respectively. Vibrational motion of a molecule results in the generation of IR spectrum. Compounds possess characteristic vibrational frequencies, hence FTIR spectroscopy is used to characterize inorganic, organic and biological molecules. Intensity of an IR band is directly proportional to the concentration of the chemical compound; thereby it can also be used for quantitative analysis [3, 9].

Michelson interferometer gives rise to FTIR spectrum. Components of FT-IR spectrophotometer include:

- Source of IR radiation
- Beam Splitter
- Two Mirrors (with coated front surfaces)
- Detector

Nernst filament is used as a source of IR radiation. Radiation produced by the source gets divided into two beams having equal intensity. One passes through the sample, while the other is used as a reference beam. Difference in the intensity of the radiation passing through both the beams gives the absorption by the sample. Mirrors reflect both beams towards an optical chopper i.e. light chopping device, which directs the beam towards the monochromator. Monochromator converts polychromatic light into monochromatic light, rotates and directs sample and reference beam onto the detector. Detector converts the thermal energy into an electrical signal, which is the amplified and obtained on a read-out device [4].

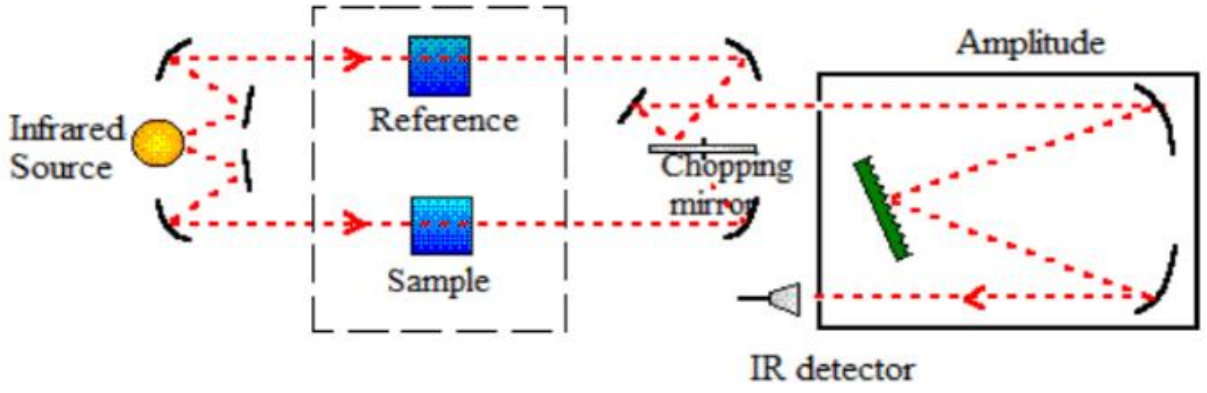

Figure 2.5 Schematic representation of FT-IR Spectrophotometer

2.8.3 Scanning Electron Microscopy (SEM)

In scanning electron microscopy, a high energy electron beam is focused over the surface of the sample in order to create an image. Electrons enter the specimen, get scattered, lose their energy and finally get absorbed. Scattering range depends upon the atomic number of elements, density of the atoms that make up the specimen and electron energy. Scattering range is directly proportional to energy, whereas it has an inverse relation with density and atomic number of the constituent atoms. In this way, a visible image is obtained. The electron beam interacts with the sample, variety of signals are produced. A selected area over the surface of sample is analyzed and data is collected, a two-dimensional image is produced, which gives information about the composition (when used with EDX), surface topography (external morphology) and orientation of the sample components. Specific points on the surface of the sample can also be analyzed by using SEM [6].

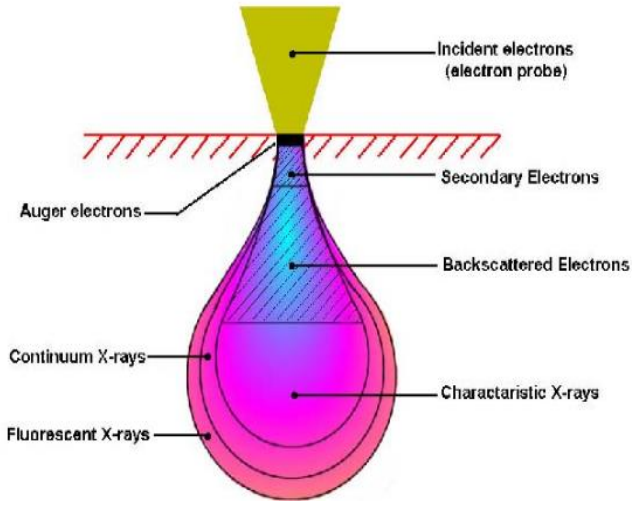

Figure 2.6 Schematic illustration of electron beam interaction in scanning electron microscopy

Essential components of a scanning electron microscope include:

- Electron probe
- Specimen stage
- Electromagnetic lens

- Secondary electron detector
- Image display unit
- Operation system

An electron gun mounted at the top of the instrument is used as a source of electrons. Two types of guns used for the generation of electrons include Field emission gun and thermionic gun. Greater the number of electrons used, greater would be the magnification obtained [9]. An electromagnetic lens, placed in the vacuum chamber, directs the electrons towards the sample. A sample stage is present in the sample compartment of a scanning electron microscope, which shows horizontal and vertical movement, rotation etc. When the incident beam interacts with the sample, backscattered electrons, secondary electrons and auger electrons are emitted. Different types of detectors are used for the detection of the ejected electrons, depending upon the type of the ejected electrons. Secondary electrons provide information about the surface topography and morphology of material, whereas backscattered electrons help to determine the distinctions in multiphase samples [5, 6].

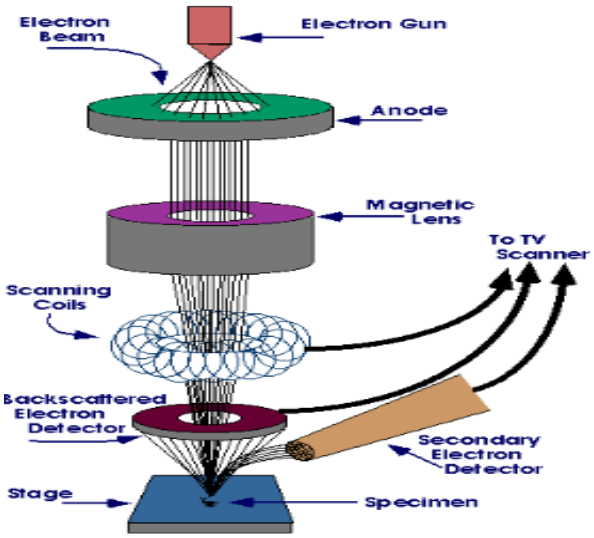

Figure 2.7 Schematic diagram of the components of scanning electron microscope

2.8.4 EDX Analysis

Energy Dispersive X-ray Spectroscopy is an analytical technique used for the qualitative as well as quantitative analysis of a material. Chemical composition of a sample, with elements having

atomic number greater than 3, can be analyzed by using EDX. Electromagnetic radiations strike with matter, and result in the emission of X-rays. Every element possesses a characteristic emission pattern because of its unique atomic structure. Atoms when at rest, are in the ground state. When a high energy beam of X-rays or electrons strike the sample, electron excites to a higher energy level, leaving behind an electron vacancy. This electron vacancy is filled by an electron from a higher energy level, and the energy difference between the higher and lower energy levels is released in the form of X-ray. Energy dispersive spectrophotometer is used to measure the released energy. Energy difference between two shells is characteristic of an element, hence in this way elemental composition of a material can be determined using energy dispersive spectrophotometer. Peak position helps in qualitative analysis of the sample, whereas peak height reflects to the concentration of a particular element in the sample. Characteristic X-rays of elements are separated by the EDX detector into an energy spectrum. An EDX Spectra is a plot between X-ray counts and energy. As each element shows a distinct X-ray absorption pattern, therefore the identification of the elements and their concentration can be estimated by EDX analysis [6].

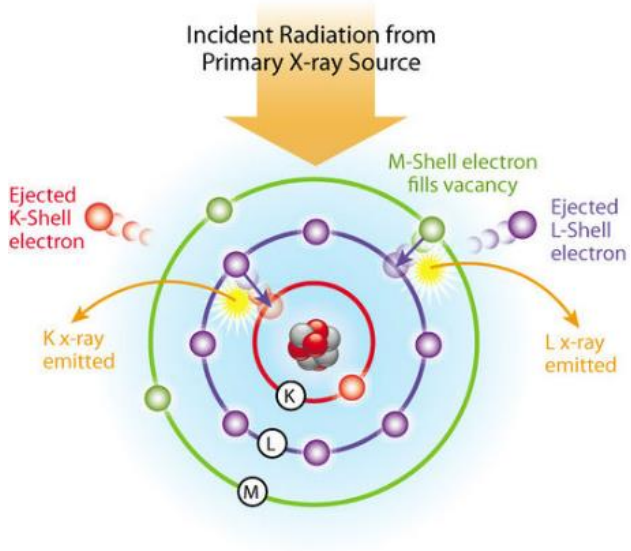

Figure 2.8 Schematic illustration of mechanism of Energy dispersive spectroscopy

Major components of an energy dispersive spectrophotometer include:

- Source of radiation

- X-ray detector
- Pulse processor
- Analyzer

2.8.5 UV-VISIBLE Analysis

This analysis provides qualitative and quantitative information about the sample. 200-400nm comprises the ultraviolet region of the electromagnetic spectrum, whereas 400nm-800nm corresponds to the visible light region of the spectrum. Analytical information is obtained in the form of transmittance, reflectance or absorbance of energy within a certain range of wavelength. The incident light on the sample has a certain energy and wavelength. Some of the light is absorbed by the sample, while the remaining is transmitted. Photo-detector measures the energy of the transmitted radiations, which in-turn gives the absorbance by the sample. UV-Vis spectroscopy involves the attenuation of beam of light, when light passes of the sample or reflects back.. Absorbance of light at a specific wavelength results in the excitation of electrons from LUMO to HOMO. Energy difference between the already occupied orbital and the orbital to which the electron is promoted corresponds to the wavelength of absorbed radiation. Several transitions occur, which result in the formation of several bands in the absorption spectrum, known as UV-Vis spectrum. A UV-Vis spectra is a plot between absorbance and wavelength, whereas UV-Vis diffuse reflectance spectra is a plot between wavelength and reflectance.

UV-Vis analysis follows Beer-Lambert law, which states that “when a monochromatic light beam passes through the solution, there comes a direct relation between rate of decrease in the intensity with thickness to the conc. of solution i.e., A=Ecl (where A=absorbance, E= absorptivity coefficient, l=path length, c=concentration of the solution). This relation is established as, transmittance refers to the ratio between transmitted light to incident light. Absorbance is the inverse of transmittance [8].

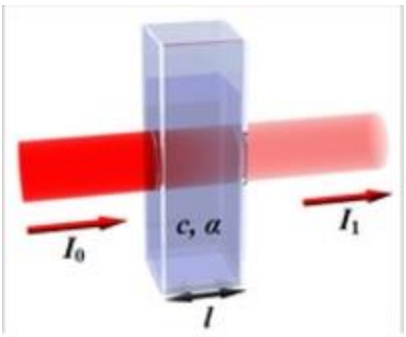

Figure 2.9 Pictorial illustration of Beer-Lambert law

Components of a UV-Vis spectrophotometer include:

- Source of light
- Monochromator
- Sample Holder
- Detector
- Processor and a read-out device

Hydrogen-deuterium discharge lamp and tungsten filament lamp are the source of light used in UV-Vis spectrophotometer. Hydrogen-deuterium discharge lamp is used for UV radiation source, whereas tungsten filament provides radiation in Visible range. Below 200nm, is the vacuum UV region. A solenoid mirror is used to reflect the ultraviolet radiations towards the monochromator. Various components of a monochromator include entrance slit, prism, exit slit, and mirrors. Prism in the monochromator converts the polychromatic light into monochromatic light. Through the exit slit, the monochromatic light beam falls on beam splitter. Beam splitter splits the light beam, one passes through the sample while the other through the reference compartment. Absorption by the sample is calculated by the difference between the intensities of light coming from the reference and sample compartment. Both beams then reflect towards the optical chopper. The chopper rotates with a frequency of 10 cycles/sec and reflects the sample and reference beam towards the detector. Photodiode is used as a detector, which converts the signal into electrical signal. This signal is then amplified and obtained at a read-out device. Absorption versus wavelength is recorded; hence it gives a UV-Vis spectrum [7, 10].

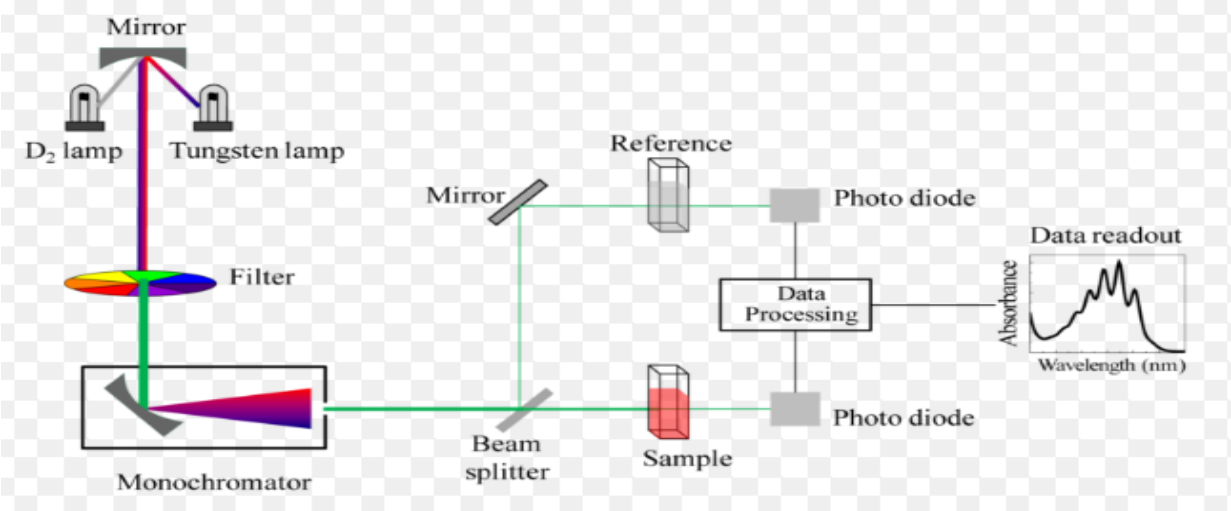

Figure 2.10 Schematic diagram of UV-Vis Spectrophotometer

2.8.6 XPS Analysis

Electron spectroscopy for chemical analysis (ESCA) is another name used for X-ray photoelectron spectroscopy (XPS). Surface chemistry of a material is analyzed by using XPS. Empirical formula, elemental composition, electronic and chemical state of elements can be determined by XPS analysis. X-rays irradiate the surface of the sample, kinetic energy is measured and the electrons emitted from 1-10nm of the sample surface are analyzed. A photoelectron spectrum is obtained between the ejected electrons and their respective kinetic energies. Atoms emit electrons of a characteristic energy and results in the formation of peaks. Thus, the intensity and energy of the peak helps to identify and quantify the elements present on the surface of the material (except hydrogen)

References

1) B. D. Cullity, Elements of X-ray Diffraction. Addison-Wesley Publishing Company, **1978**.

2) K. R. Hebbar, Basics of X-Ray Diffraction and its Applications. I. K. International Publishing House Pvt. Limited, **2007**

3) H. W. Siesler, Y. Ozaki, S. Kawata and H. M. Heise, eds. Near-Infrared Spectroscopy: Principles, Instruments, Applications. John Wiley & Sons, **2008**
4) Stuart, Barbara. Infrared Spectroscopy. John Wiley & Sons, Inc., **2005**

5) J. Goldstein. Scanning electron microscopy and x-ray microanalysis. Kluwer Academia/Plenum Publishers, **2003**

6) R. F. Egerton. Physical principles of electron microscopy: an introduction to TEM, SEM, and AEM. Springer, **2005**.

7) H. H. Perkampus, Encyclopedia of Spectroscopy. Weinheim; New York: VCH, © **1995**

8) H. H. Perkampus, UV/VIS Spectroscopy and its Applications. Springer, Berlin, Heidelberg

9) A. R. Clarke, Microscopy techniques for materials science. CRC Press (electronic resource), **2002**

10) B. J. Clark, T. Frost and M. A. Russell. UV Spectroscopy: Techniques, Instrumentation, Data handling. London; New York: Chapman & Hall, **1993.**

$Co_3V_2O_8$/ $Zn_3V_2O_8$ Nanocomposites

Abstract

Chemical composites of $Co_3V_2O_8$ and $Zn_3V_2O_8$ have been synthesized in different molar ratios via co-precipitation method. These nanocomposites find various photocatalytic applications, while here the main focus is on environmental applications. The as-synthesized material was characterized using different techniques, in order to confirm the crystal structure, lattice parameters, morphology, elemental composition and optical properties etc.

3.1 Structural Analysis

XRD verifies the crystal structure and purity of the synthesized material. In case of bare $Zn_3V_2O_8$, diffraction pattern is found to be in accordance with a reported pattern, (JCPDS no.00-034-0378), which confirms the synthesis of the orthorhombic $Zn_3V_2O_8$. No extra peak has been observed, which contributes to the purity of the product. In XRD pattern of $Co_3V_2O_8$ nanostructures, most of the reflection peaks are attributed to the orthorhombic phase $Co_3V_2O_8$, in accordance with Joint Committee on Powder Diffraction Standards (JCPDS card No. 74-1486). Material is said to be pure, as no extra peaks have been observed. Hence, XRD patterns of synthesized $Co_3V_2O_8$ and $Zn_3V_2O_8$, are found to have a good match with those already reported. $Zn_3V_2O_8$ seems to possess sharp peaks in comparison with $Co_3V_2O_8$, which reflects towards high crystallinity of the former photocatalyst. In order to obtain higher efficiency for photocatalytic dye degradation, $Co_3V_2O_8$ and $Zn_3V_2O_8$ have been combined in various molar ratios. In **Fig 3.1** different composites of $Co_3V_2O_8$ and $Zn_3V_2O_8$ tend to show an exact match with the diffraction peaks of bare $Co_3V_2O_8$ and bare $Zn_3V_2O_8$. XRD pattern confirms the formation of nanocomposites of $Co_3V_2O_8/Zn_3V_2O_8$, as all the peaks from $Co_3V_2O_8$ and $Zn_3V_2O_8$ are present in the composite. Intensity of 311 peaks corresponding to $Zn_3V_2O_8$, is increasing with the increase in concentration of $Zn_3V_2O_8$ in the composites.

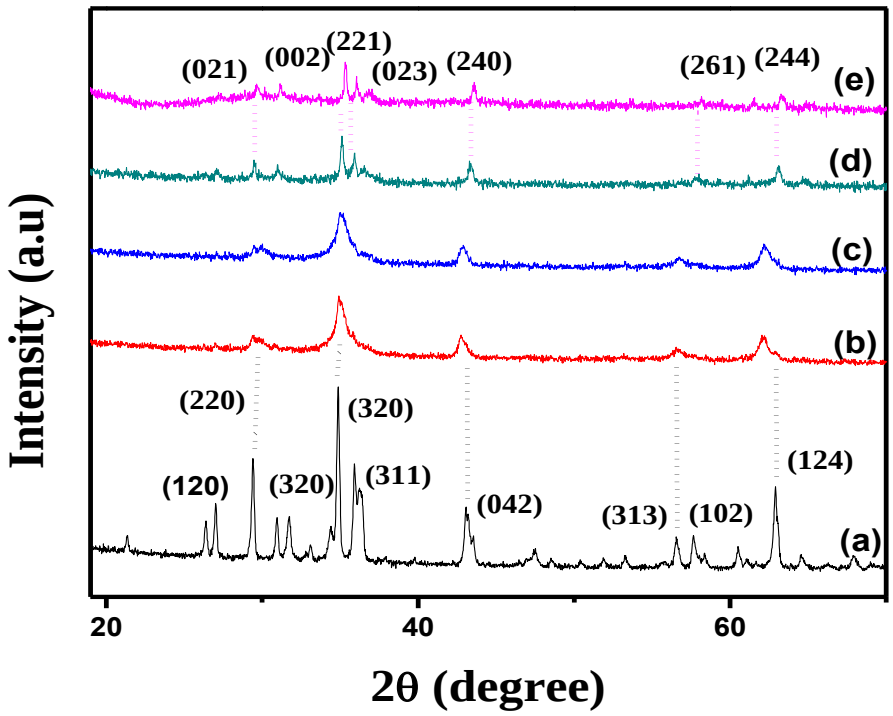

Figure 3.1 XRD pattern of (a) $Zn_3V_2O_8$ (b) 28mM $Zn_3V_2O_8$ (c) 25mM $Zn_3V_2O_8$ (d) 10mM $Zn_3V_2O_8$ (e) $Co_3V_2O_8$

Table 3.1 XRD data of prepared samples

Sample	Crystallite Size (D) (nm)	Lattice constant (a) (Å) Å	Cell Volume (V) (A_3)
$Co_3V_2O_8$	62.6	4.2341	277.7
$Zn_3V_2O_8$	117	8.2990	584.7

Crystallite size (D), cell volume (V) and lattice constant (a) of $Co_3V_2O_8$ and $Zn_3V_2O_8$ have been calculated, using the XRD data as shown in **Table 3.1.** Scherrer formula is used to calculate the crystallite size (eq. 1), whereas eq. 2 and eq. 3 have been used to calculate the cell volume and lattice constant. All the results are in good accordance with the reported data.

$$D = K\lambda/\beta\cos\theta \quad (1)$$

$$1/d2 = (h2 + k2 + l2)/a2 \quad (2)$$

$$V = a3 \quad (3)$$

3.2 Morphological and EDX Analysis

SEM has been used for the morphological analysis of the synthesized photocatalysts, as shown in **Fig. 3.2**. **Figure 3.2(a)** shows that, $Zn_3V_2O_8$ possesses agglomerated spherical morphology, exhibiting size within a range of 55-60nm. **Fig. 3.2(e)** presents the coral like morphology of $Co_3V_2O_8$ nanoparticles having a size of around 50nm. Nanocomposite with 2Mm $Co_3V_2O_8$ and 28Mm $Zn_3V_2O_8$ show well dispersed spherical $Zn_3V_2O_8$ over slight coral sheets of $Co_3V_2O_8$. **Fig. 3.2(c)** shows a uniform deposition of spherical $Zn_3V_2O_8$ over flat coral sheets of $Co_3V_2O_8$. With the increase in the concentration of $Co_3V_2O_8$ as shown in **fig. 3.2(e)**, spherical morphology vanishes, leaving behind coral like morphology.

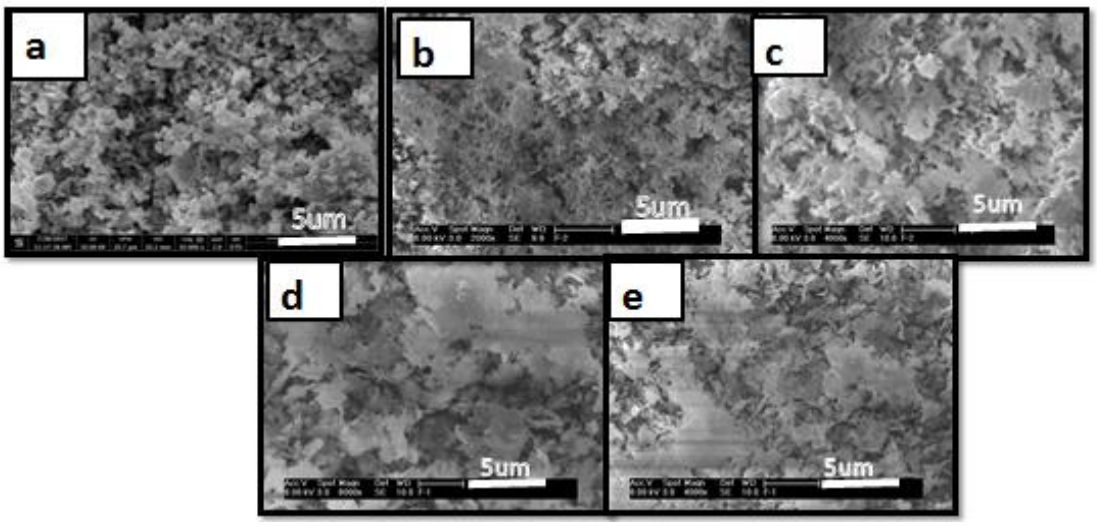

Figure 3.2 SEM images of (a) $Zn_3V_2O_8$, (b-d) $Co_3V_2O_8/Zn_3V_2O_8$ nanocomposites with 28mM, 25mM and 10Mm $Zn_3V_2O_8$respectively, and (e) $Co_3V_2O_8$

3.3 Compositional Analysis

EDX analysis has been carried out in order to determine the stoichiometry and elemental composition, as shown in **Fig. 3.3**. All the peaks present in **Fig. 3.3(a)** corresponds to Zn, V and O, which confirms the purity of the synthesized material. Similarly Fig. 3.3(b) clearly shows the

presence of Co, V and O in the EDX spectrum, depicting high purity of the product. **Fig 3.3(c-e),** shows that the elements present in the material include Co, Zn, V, O. These results clearly show that all the components present in the composites are in accordandance with the desired stoichiometric proportions.

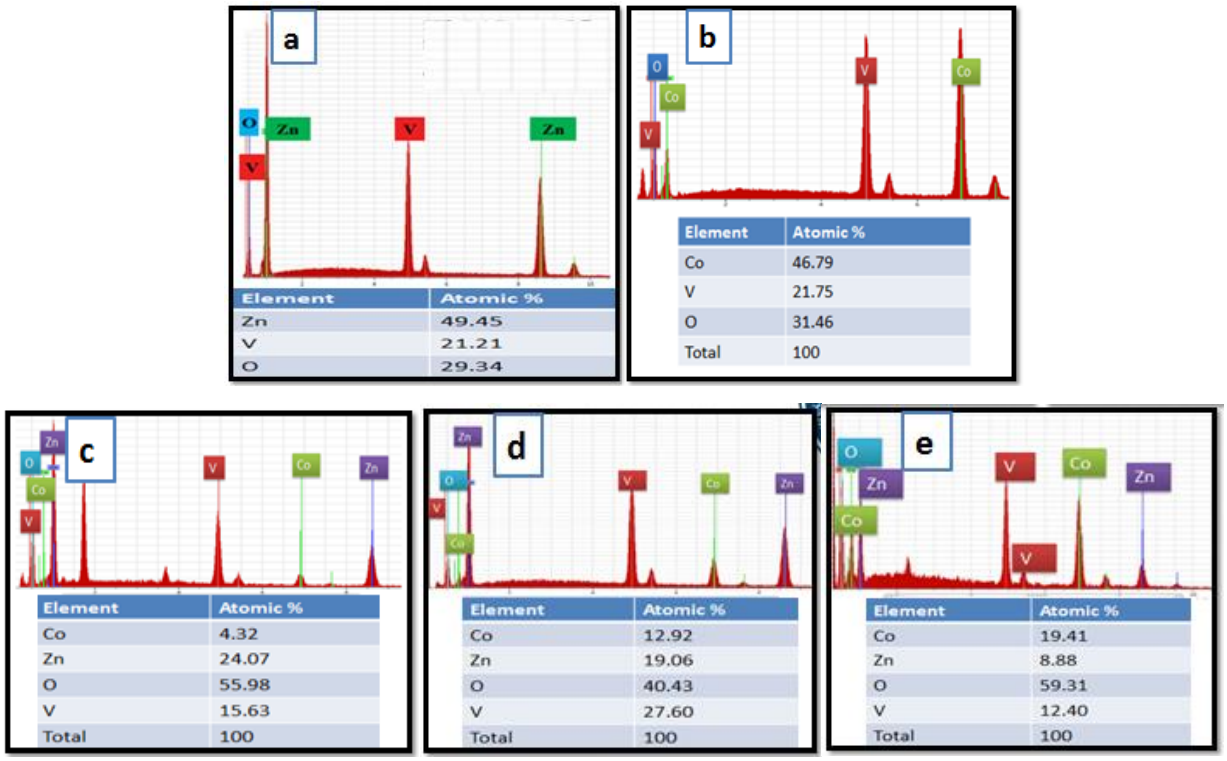

Figure 3.3 EDX elemental composition of (a) $Zn_3V_2O_8$ (b) $Co_3V_2O_8$ nanocomposites with different amount of $Co_3V_2O_8$ (c) 2mM (d) 5mM (e) 20mM

Energy Dispersive X-ray (EDX) elemental mapping shows the elemental distribution and composition of the synthesized material. **Fig. 3.4(a)** also helped to determine the composition and elemental distribution of synthesized material. **Fig. 3.4(a)** shows the elemental map ofbare $Zn_3V_2O_8$, **Fig. 3.4(b)** depicts the elemental mapping for $Co_3V_2O_8$, which clearly shows well dispersed Co,V and O in the synthesized material. **Fig. 3.4(c)** shows the uniform distribution of all elements present in the nanocomposite, according to their molar ratios. Here, concentration of Co is greater in the as-synthesized material, which is evident from the elemental map. Similarly nanocomposites **[(fig. 3.4(d-e))]** also confirm the presence of all the elements in required stoichiometric ratios.

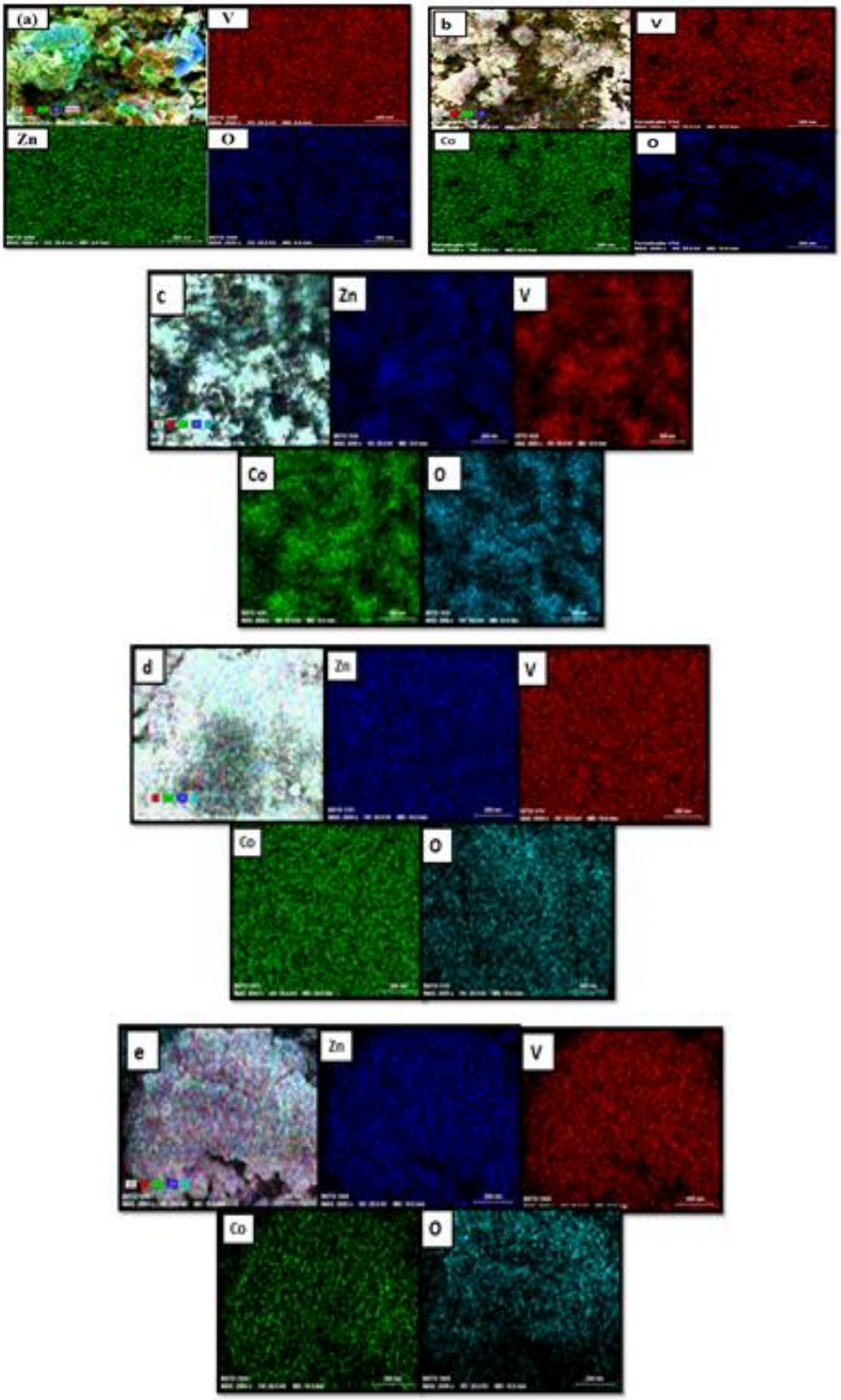

Figure 3.4 EDX Elemental mapping of $Co_3V_2O_8/Zn_3V_2O_8$

3.4 Ultraviolet-Visible Diffuse Reflectance Spectroscopy

Identification of the photocatalytic properties of a catalyst is carried out with the arrangement of its band energy levels. Band-gap and optical properties of $Co_3V_3O_8$ and $Zn_3V_2O_8$ have been determined via UV-Vis diffuse reflectance spectroscopy, (DRS). **Fig. 3.5(a)** shows the UV/Vis. diffuse reflectance spectrum of $Zn_3V_2O_8$. Band gap of $Zn_3V_2O_8$ is calculated via Tauc plot and is found to be 3.2 eV**.** UV/Vis DRS encompasses reflectance factor, F(R) rather than absorption factor and it is calculated via Kubelka-Munk expression as shown in equation (1).

$$F(R) = \frac{(1-R)^2}{2R} = K/S \qquad (1)$$

Where R is absolute reflectance, K is Molar absorption co-efficient and S is scattering co-efficient.

A UV/Vis DRS spectrum of $Co_3V_2O_8$ is shown in **Fig. 3.5(b)**, which clearly indicates that $Co_3V_2O_8$ show strong absorption in blue region of the solar spectrum ~at 565nm. Kubelka-Munk function is utilized to change the diffuse reflectance spectrum to equivalent absorption coefficient. Optical band gap of $Co_3V_2O_8$ was found to be 2.19eV by means of Tauc plot.

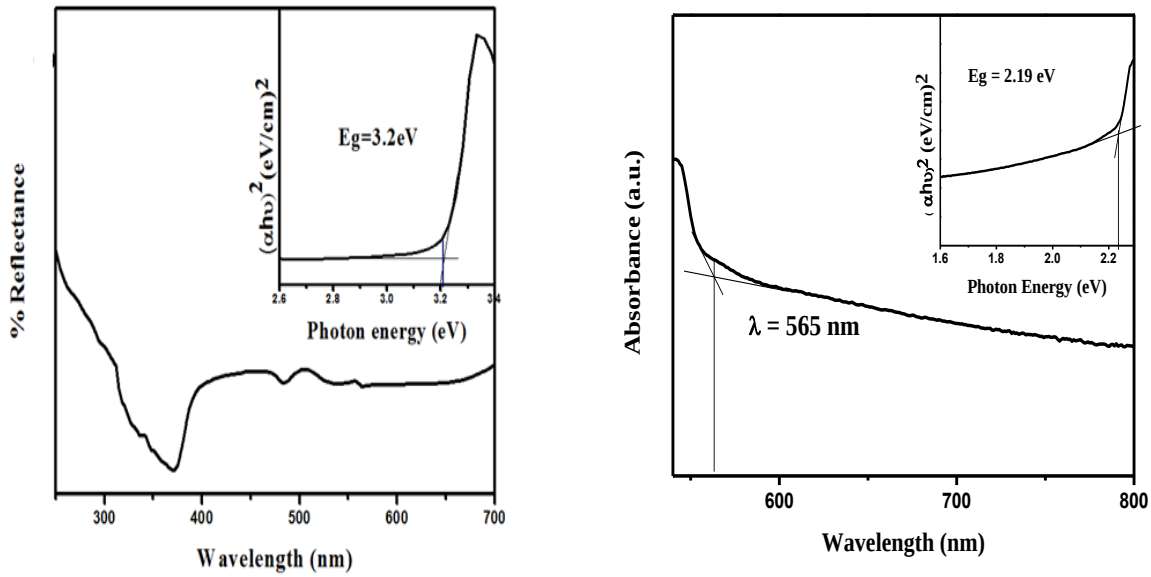

Figure 3.5 (a) UV-Vis spectrum of $Zn_3V_2O_8$ **(b)** UV-Vis spectrum and Tauc plot of $Co_3V_2O_8$

3.5 Photocatalytic Activity Mechanism

The percentage degradation of Congo red as a function of time by using $Co_3V_2O_8$, $Zn_3V_2O_8$ and their composites is shown in **Fig. 3.6.** Following equation was used to calculate the % degradation of Congo red.

$$\eta = \frac{C_\circ - C_t}{C_\circ} \times 100\ (\%)$$

Here,

Co=initial concentration and Ct= Concentration of dye at time t

$Co_3V_2O_8$ has a narrow band-gap, so it can easily be excited by visible light. Upon excitation, charge carriers are produced. Electrons from the conduction band of $Co_3V_2O_8$ get transferred to the Conduction band of $Zn_3V_2O_8$, leaving behind holes in the valence band of $Co_3V_2O_8$. Successful separation of charge carriers results in the improvement of photocatalytic efficiency of the photocatalyst. Holes in the valence band combine with water and generate H^+ and OH, whereas the electrons present in the conduction band result in the generation of $O^{2\cdot-}$ (superoxide) radical, which further reacts with water and forms $OH^{\cdot}$ radical. These radicals carry out the degradation of organic dyes

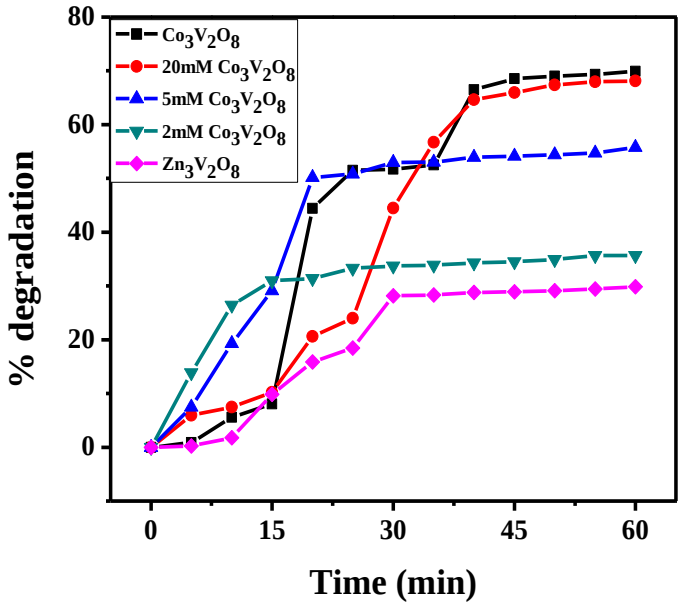

Figure 3.6 % degradation of Congo red as a function of time

Fig. 3.6 shows the photocatalytic degradation of congo red by bare $Co_3V_2O_8$, bare $Zn_3V_2O_8$ and their nanocomposites. Dye degradation studies have been carried out up to 60 min. Bare $Zn_3V_2O_8$ showed a gradual increase in the % dye degradation for the first 30 min. After that, the activity of the catalyst became constant with 28% degradation. Similarly, bare $Co_3V_2O_8$ showed excellent results for dye degradation, and even after 60 min, the photocatalyst showed an increase in the efficiency. 69% dye was degraded after first 60 min. Composite with the least content of $Co_3V_2O_8$ i.e. 2mM showed around 30% dye degradation in the first 5 min, after that the efficiency of the material vanished. Composite with 5mM $Co_3V_2O_8$ showed a maximum of 45% degradation, whereas composite with 20Mm $Co_3V_2O_8$ showed maximum photocatalytic activity i.e around 69%. Less % degradation in case of 2mM and 5mM nanocomposites can be attributed to the blockage of active sites in the photocatalyst.

References:

1) F. Mazloom, M. M. Arani and M. S. Niasari, *Journal of Material Sciences and Material Electronics*, **2016**, 27, 1974-1982

2) M. G. Arani, M. M. Arani and M. Niasari, *Journal of Molecular Catalysis A: Chemical*, **2016**, 425, 31-42

3) J. Liu, Y. Wang and D. Sun, *Journal of Renewable Energy*, **2012**, 38, 214-218

4) Dong, Z. Du, Y. Zhao and D. Zhou, *Powder Technology*, **2010**, 198, 32

$Co_3V_2O_8$/ g-C_3N_4Nanocomposites

Abstract

Different weight percent (25%, 50% and 75%) of $Zn_3V_2O_8$ have been combined with g-C_3N_4 to form heterostructures in order to attain enhanced photocatalytic applications. This chapter incorporates the characterization of the synthesized photocatalyst and its photocatalytic application in the removal of environmental pollutants. A detailed explanation of the synthesis and purity of the as-synthesized photocatalyst has been discussed here, depicting the morphology, crystallite size, %age composition of $Co_3V_2O_8$/ g-C_3N_4 nanocomposites.

4.1 Structural Analysis

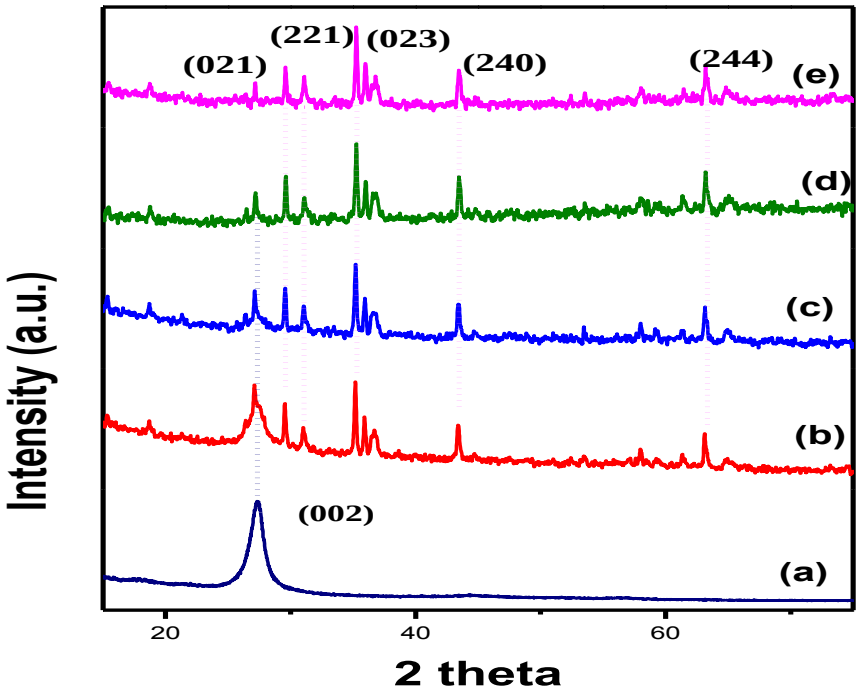

Figure 4.1 XRD pattern of (a) g-C_3N_4 (b) 25% g-C_3N_4 (c) 50% g-C_3N_4 (d) 75% g-C_3N_4 (e) $Co_3V_2O_8$

XRD analysis has been carried out to determine the crystal structure of $Co_3V_2O_8$/g-C_3N_4 photocatalyst **(Fig. 4.1).** In case of bare $Co_3V_2O_8$ **[Fig. 4.1(e)]**, XRD has confirmed the orthorhombic geometry and phase purity which is in accordance with the standard available data (PDF # 74-1486). **Fig. 4.1(a)** shows that the diffraction peaks in the as-synthesized material are in accordance with the reported diffraction pattern for g-C_3N_4, which shows a good match with the standard diffraction pattern (JCPDS file no. 15-0746). Cubic g-C_3N_4, with a sharp peak at $2\theta=27.5^o$, and no extra peak confirms the purity of the product. In both samples, no extra peak of impurity has been observed. **Fig. 4.1(b)** shows the XRD pattern of composite with 75% g-C3N, **Fig. 4.1(c)** is 50% g-C_3N_4 and **Fig. 4.1(d)** has 25% g-C_3N_4. Sharp peaks obtained in case of $Co_3V_2O_8$ show that the material is crystalline in nature. Diffraction pattern of different composites of $Co_3V_2O_8$ and g-C_3N_4, ensures the formation of desired photocatalyst. Intensity of the peak at 27.5^o is highest in the composite having 75% g-C_3N_4, as shown in **Fig. 4.1(b).** With the decrease in the concentration of g-C_3N_4 in the as-synthesized photocatalyst, a decrease in the peak intensity is observed, as evident from **Fig.4.1(c-d)**. All the peaks from $Co_3V_2O_8$ and g-C_3N_4 are present in all the composites. Similarly, the characteristic peaks in $Co_3V_2O_8$ are most evident in the photocatalyst having 75% $Co_3V_2O_8$ **[Fig. 4.1(d)]**, and a gradual decrease in the intensities is observed with the decrease in relative amount of $Co_3V_2O_8$.

Crystallite size (*D*), lattice constant (*a*) and cell volume (*V*) for $Co_3V_2O_8$ and g- C_3N_4 have been calculated by using XRD data as shown in **Table 4.1.** Scherrer formula was used to calculate the crystallite size (**equation 1**) while lattice constant was calculated using **equation 2** and cell volume by **equation 3**. All the calculated parameters are in good agreement with the reported data.

$$D = K\lambda/\beta cos\theta \qquad (1)$$

$$1/d^2 = (h^2 + k^2 + l^2)\ /a^2 \qquad (2)$$

$$V = a^3 \qquad (3)$$

Table 4.1 XRD data of prepared composites

Sample	Crystallite Size (D) (nm)	Lattice constant (a) (Å)	Cell Volume (V) (A_3)
$Co_3V_2O_8$	62.6	4.2341	277.7
g-C_3N_4	29.4	2.3681	109.771

4.2.Morphological Analysis

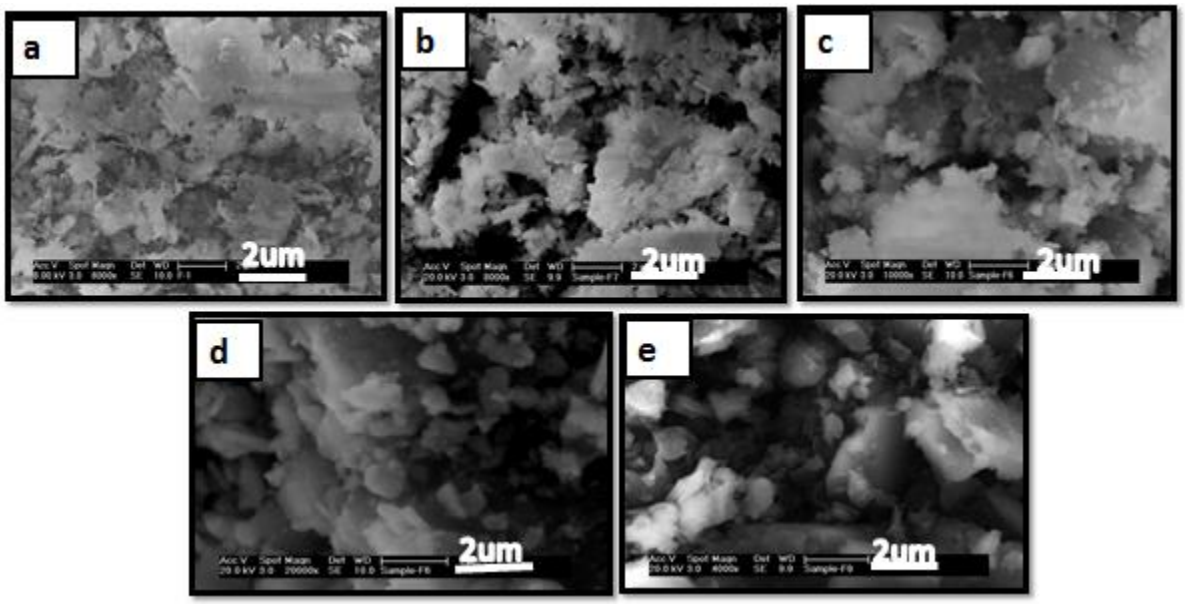

Figure 4.2 SEM analysis of (a) bare $Co_3V_2O_8$ (b) 25% $Co_3V_2O_8$ (c) 50% $Co_3V_2O_8$ (d) 75% $Co_3V_20_8$ (e) bare g-C_3N_4

Fig. 4.2 shows the morphological analysis for the synthesized photocatalysts, using SEM. Fig. **4.2(a)** shows that bare $Co_3V_2O_8$ possesses coral like morphology with a uniform size distribution in the range of 50-55nm. Bare g-C_3N_4 has a rod like morphology, as evident from Fig. **4.2(e)**. Nanocomposite with 25% g-C_3N_4 **[Fig. 4.2(b)]** clearly shows highly agglomerated coral like $Co_3V_2O_8$ nanostructures over rod like g-C_3N_4. As the amount of g-C_3N_4 increases **[Fig.4.2(c)],** layer of coral like $Co_3V_2O_8$ is seen over the g-C_3N_4 structure. Upon further increase in the amount of g-C_3N_4 up to 75%, well dispersed $Co_3V_2O_8$ coral structures over the surface of the rod like g-C_3N_4 is seen, as shown in **Fig. 4.2(d)**.

4.3 Compositional Analysis

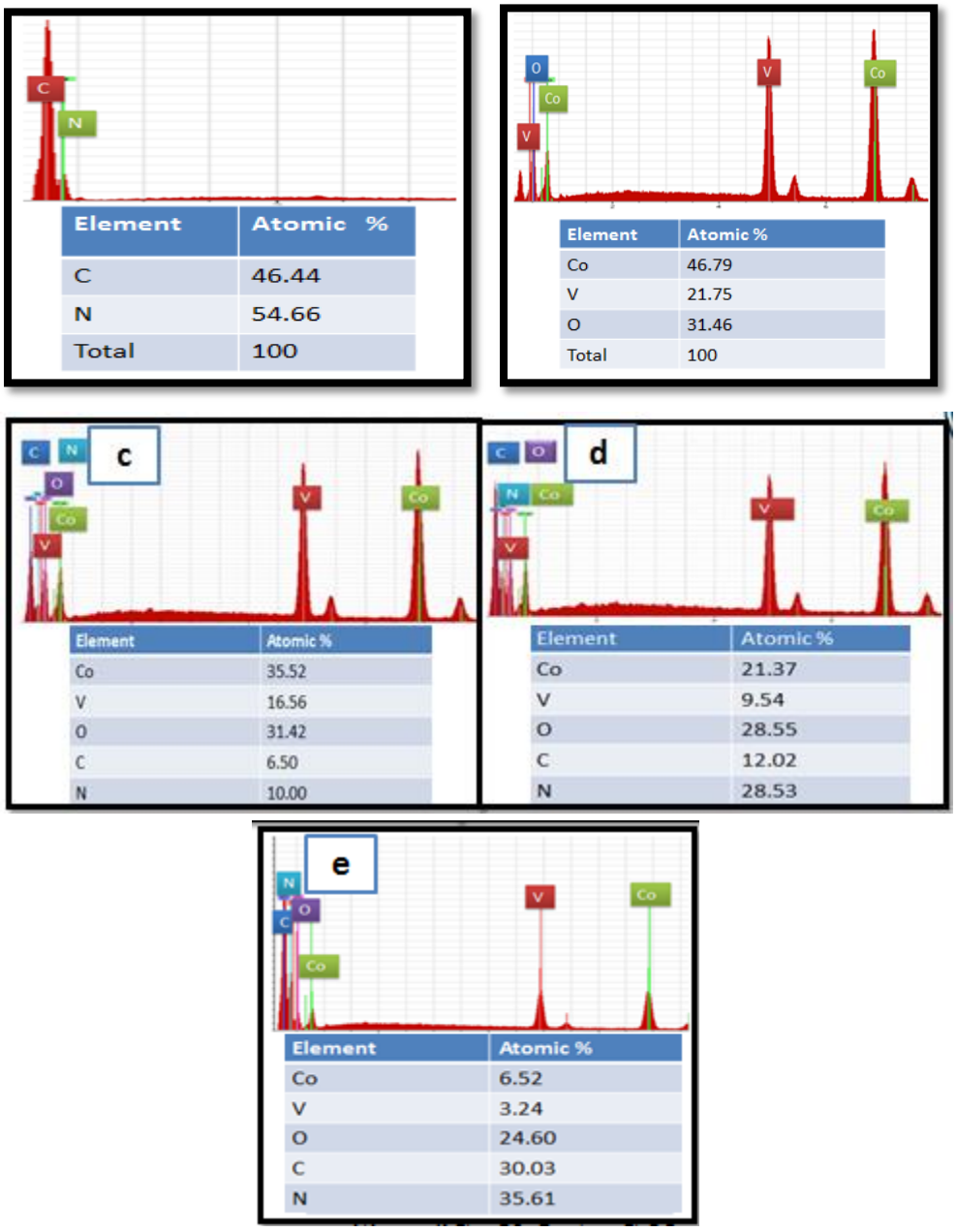

Figure 4.3 EDX elemental composition of (a) bare g-C_3N_4 (b) bare $Co_3V_2O_8$ (c) 75% g-C_3N_4 (d) 50% g C_3N_4 (e) 25% g-C_3N_4

Fig. 4.3 shows the elemental analysis and the stoichiometric ratios of the synthesized photocatalysts determined via EDX analysis. These results clearly show that all the elements in the bare material as well as the composite are in accordance with desired stoichiometric ratios. **Fig. 4.3(a)** shows the presence of only C and N in bare $g\text{-}C_3N_4$, which confirms the purity of the photocatalyst. Similarly, **Fig. 4.3(b)** confirms the presence of Co, V and O in the synthesized photocatalyst. **Fig. 4.3(c-e)**, shows the presence of all the elements in the nanocomposites in desired stoichiometric ratios. Composite with 75% $Co_3V_2O_8$ contains the maximum content of Co, and the amount decreases with the increase in the concentration of $g\text{-}C_3N_4$.

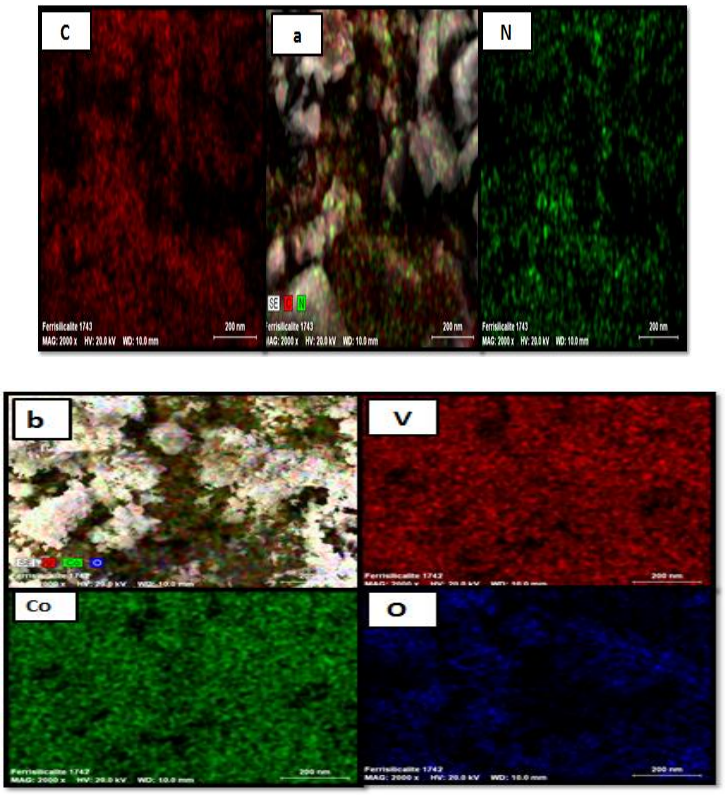

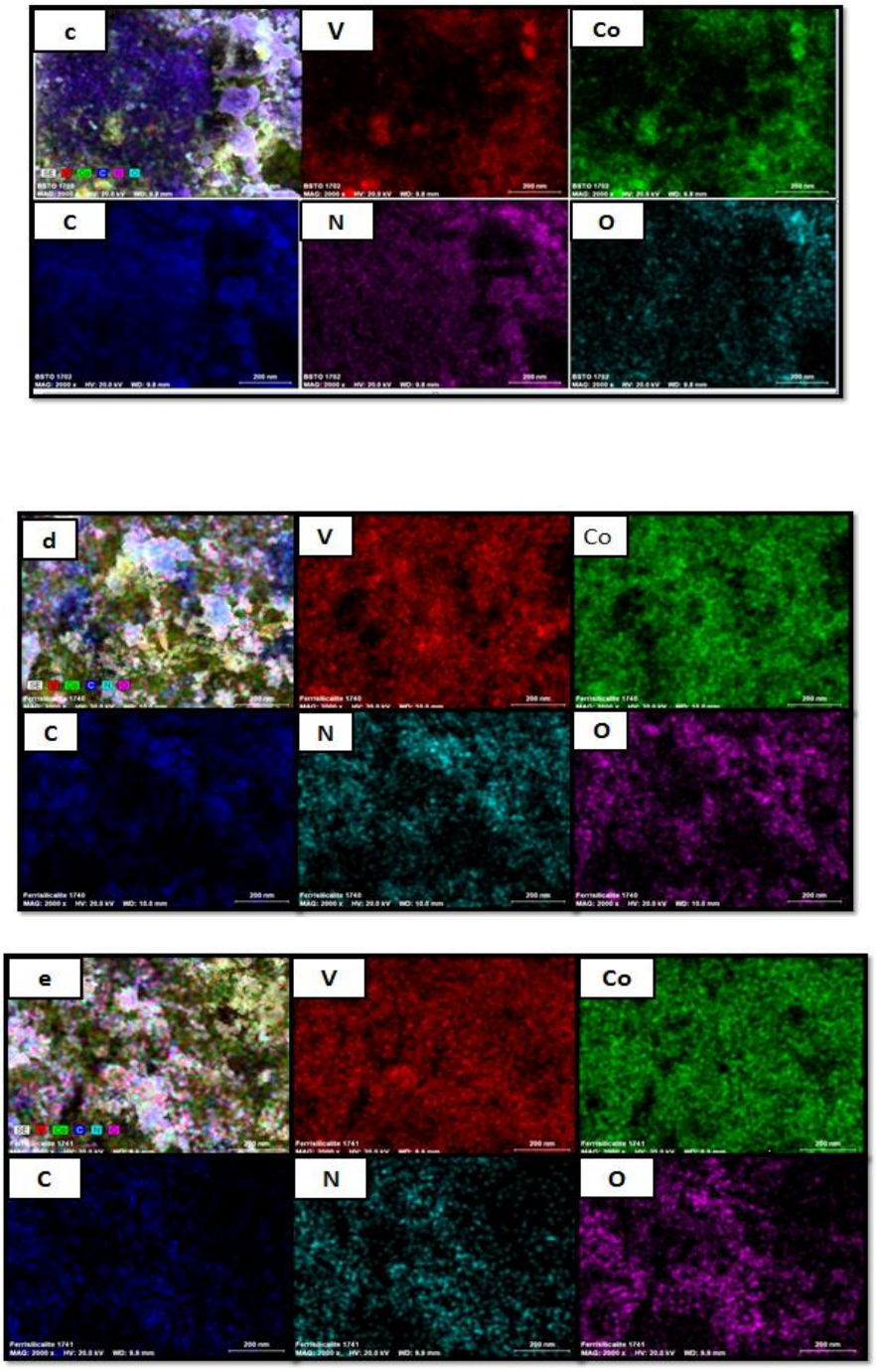

Figure 4.4 EDX Elemental mapping of $Co_3V_2O_8$/ *g-C_3N_4* (a) g-C_3N_4 (b) $Co_3V_2O_8$ & with varying amount of $Co_3V_2O_8$: (c) 25% (d) 50% (e) 75% respectively

EDX elemental mapping confirms the elemental composition and purity of as-synthesized material, as shown in **Fig. 4.4**. **Fig. 4.4(a)** shows well dispersed C and N in g-C_3N_4. Similarly Co, V and O can be mapped in **Fig. 4.4(b). Fig. 4.4(c)** with 25% $Co_3V_2O_8$ depicts the formation

of $Co_3V_2O_8$ by g-C_3N_4 acting as the base material with C and N distributed uniformly all over the surface. $Co_3V_2O_8$ nanoparticles have been well dispersed with g-C_3N_4. Results of EDX elemental mapping for composites with 50% and 75% $Co_3V_2O_8$ are also in accordance with the already mentioned discussion and conclusion.

4.4 Ultraviolet-Visible Spectroscopy

UV-Vis spectroscopy is used to study the optical properties of a material, determine its band-gap and depict the suitability of material as a photocatalyst. **Fig. 4.5** shows the UV-Vis spectrum of as-synthesized g-C_3N_4. The photocatalyst shows strong absorption at 480nm. Optical band-gap of g-C_3N_4 was found to be 2.63eV.

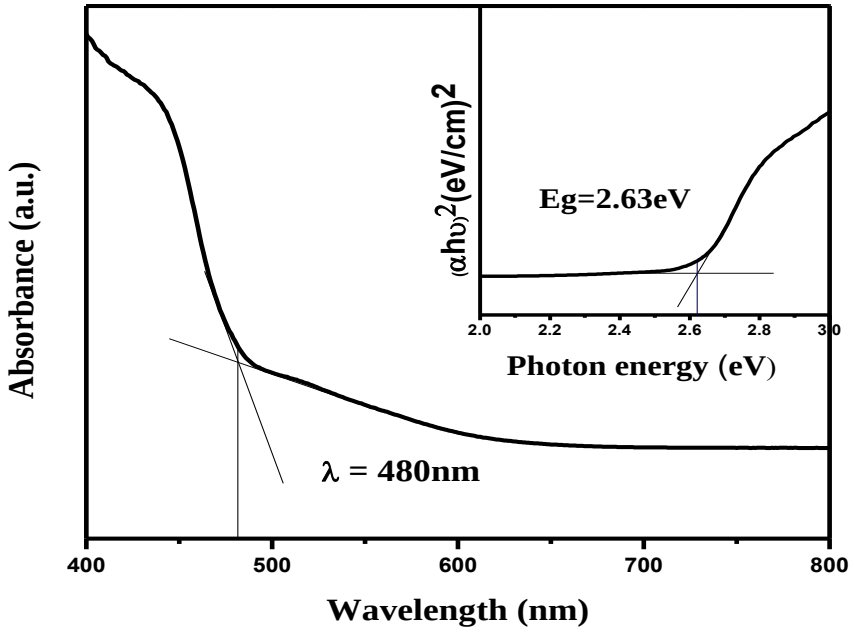

Figure 4.5 UV-Vis spectrum of g-C_3N_4

4.5 Photocatalytic Activity Mechanism

The percentage degradation of Congo red as a function of time by using $Co_3V_2O_8$, g-C_3N_4 and their composites is shown in **Fig. 4.6.** Following equation was used to calculate the % degradation of Congo red.

$$\eta = \frac{C_\circ - C_t}{C_\circ} \times 100\ (\%)$$

Here,

C_o=initial concentration and C_t= Concentration of dye at time t

$Co_3V_2O_8$ has a narrow band-gap, so it can easily be excited by visible light. Upon excitation, charge carriers are produced. Electrons from the conduction band of $Co_3V_2O_8$ get transferred to the Conduction band of g-C_3N_4, leaving behind holes in the valence band of $Co_3V_2O_8$. Successful separations of charge carriers result in the improvement of photocatalytic efficiency of the photocatalyst. Holes in the valence band combine with water and generate H^+ and OH, whereas the electrons present in the conduction band result in the generation of $O^{2\cdot-}$ (superoxide) radical, which further reacts with water and forms $OH^{\cdot}$ radical. These radicals carry out the degradation of organic dyes.

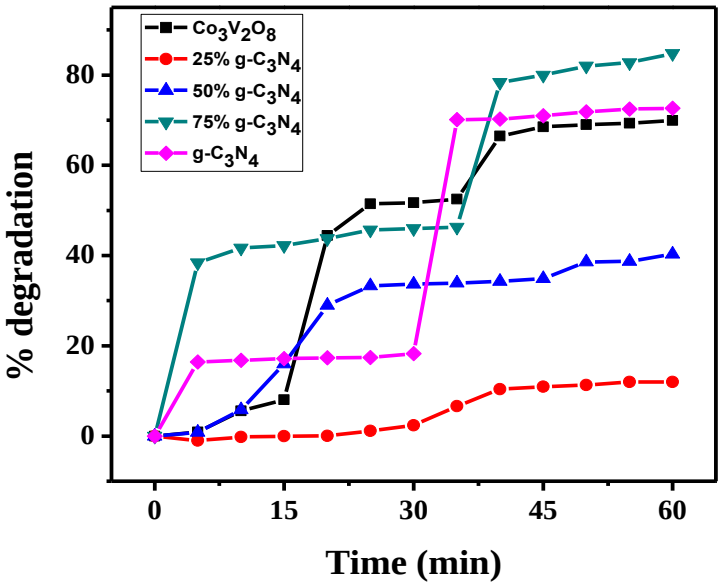

Figure 4.6 % degradation of Congo red as a function of time

Fig. 4.6 shows the photocatalytic degradation of Congo red by bare $Co_3V_2O_8$, bare g-C_3N_4 and their nanocomposites. Both the materials are efficient photocatalysts and show enhanced dye degradation. Bare $Co_3V_2O_8$ showed 65% degradation of Congo red after 40 min. At 20 min, it is the photocatalyst with maximum efficiency, whereas bare g-C_3N_4 showed a rapid increase in the photocatalytic dye degradation after 30 min and reacsshed a maximum efficiency of 70%. Composite with 25% g-C_3N_4 exhibited least efficiency. Composite with 50% of each photocatalyst showed a maximum degradation of 30%. Whereas, composite with 75% g-C_3N_4 possessed the maximum % degradation of Congo red. This might be possible because of the formation of heterostructures, which in-turn decreases the decreases the recombination rate by increasing the charge separation, thereby making more electrons and holes available to carry out the redox reactions.

References

1) M. G. Arani, M. M. Arani and M. Niasari, *Journal of Molecular Catalysis A: Chemical*, **2016**, 425, 31-42

2) X. Li, J. Zhang, L. Shen, Y. Ma, W. Lei, Q. Cui and G. Zou, *Applied Physics A*, **2009**, 94, 387-392

3) M. Wang, Y. Shi and G. Jiang, *Materials Letters*, **2014**, 122, 66-69

4) J. Tauc, R. Grigorovici and A. Vancu, *Physica Status Solidi B,* **1966**, 15, 627–639

Summary and Outlook

During this work, $Co_3V_2O_8/Zn_3V_2O_8$ and $Co_3V_2O_8/g\text{-}C_3N_4$ nanocomposites have been successfully synthesized with high efficiency for photocatalytic dye degradation. Different strategies were opted for the enhancement of photocatalytic activity i.e. synthesis of nanocomposites and heterostructure formation etc. Highlights of the research work carried out are summed up as follow:

5.1 Highlights

- $Co_3V_2O_8$ and $Zn_3V_2O_8$ photocatalysts have been successfully synthesized via co-precipitation method.
- $g\text{-}C_3N_4$ has been successfully synthesized via thermal decomposition method.
- Nanocomposites of $Co_3V_2O_8/Zn_3V_2O_8$ have been prepared in different molar ratios i.e. $Co_3V_2O_8$ 2Mm, 5mM and 20Mm respectively.
- % efficiency of $Co_3V_2O_8/Zn_3V_2O_8$ photocatalysts have been measured against photocatalytic degradation of Congo red.
- Successful combination of $Co_3V_2O_8$ with different weight % of $g\text{-}C_3N_4$ i.e. 25%, 50% and 75% has been carried out by physical method.
- Composite comprising 75% $g\text{-}C_3N_4$ and 25% $Co_3V_2O_8$ has proved to be the most efficient photocatalyst with % degradation of up to 80%
- Both of the photocatalyst combinations have proved to be efficient towards the removal of water pollutants.
- Heterostructure formation is confirmed by FTIR, UV-Vis, XRD, SEM and EDX.

5.2 Future Perspectives

Photocatalytic degradation of environmental pollutants is a cost effective approach towards the removal of toxic and carcinogenic materials. Future goals include to increase the efficiency of $Co_3V_2O_8/Zn_3V_2O_8$ nanocomposites by controlling different reaction parameters. We should also focus on making the photocatalyst Visible light active, so that it absorbs more range of the solar spectrum. Different factors that can contribute towards increasing the photocatalytic efficiency are as below:

- Computational studies along with the experimental techniques can help us devise a better strategy towards the synthesis of photocatalysts.
- Efficient strategies should be developed in order to enhance the charge separation, increase surface area through nanostructuralization and increase the surface active sites for photocatalysis.
- $Co_3V_2O_8/Zn_3V_2O_8$ and $Co_3V_2O_8/g\text{-}C_3N_4$ composites can be used for other photocatalytic applications i.e. H_2 production, CO_2 reduction etc.